Haffner-Staton, Ephraim and Balahmar, Norah and Mokaya, Robert (2016) High yield and high packing density porous carbon for unprecedented CO2 capture from the first attempt at activation of air-carbonized biomass. Journal of Materials Chemistry, 4 (34). pp. 13324-13335. ISSN 1364-5501

# High yield and high packing density porous carbon for unprecedented $CO_2$ capture from the first attempt at activation of *air-carbonized* biomass

Ephraim Haffner-Staton, Norah Balahmar, Robert Mokaya*

School of Chemistry, University of Nottingham, University Park, Nottingham NG7 2RD, U. K.

*Corresponding author. E-mail: r.mokaya@nottingham.ac.uk (R. Mokaya)

## Abstract

The first attempt at activation of air-carbonized carbon reveals unusual resistance to activation and unprecedentedly high yields (32 – 80 wt%) of high packing density (0.7 – 1.14 g $cm^{-3}$) microporous carbon dominated by 5.5 – 7 Å pores, which are just right for $CO_2$ uptake (up to 5.0 mmol $g^{-1}$) at 1 bar and 25 $^oC$. The high gravimetric uptake and packing density offer exceptional volumetric storage, and unprecedented performance for low pressure swing adsorption (PSA) with working capacity of 6 – 9 mmol $g^{-1}$ for a pure $CO_2$ stream (6 to 1 bar) and 3 – 4 mmol $g^{-1}$ for flue gas (1.2 to 0.2 bar). The working capacity for vacuum swing adsorption (VSA) is attractive at 5.0 – 5.4 mmol $g^{-1}$ under pure $CO_2$ (1.5 to 0.05 bar), and 1.8 – 2.2 mmol $g^{-1}$ for flue gas (0.3 to 0.01 bar). The pure $CO_2$ volumetric working capacity breaks new ground at 246 – 309 g $l^{-1}$ (PSA) and 179 – 233 g $l^{-1}$ (VSA). For flue gas conditions, the working capacity is 120 to 160 g $l^{-1}$ (PSA). The performance of the activated air-carbonized carbons is higher than the best carbons and benchmark zeolites or MOFs.

## 1. Introduction

On the 12th of September 2014, a fire destroyed the University of Nottingham's partially constructed all-wood Carbon Neutral Laboratory (CNL). Since this tragic happening, work commenced anew on building the UK's first carbon neutral lab, which was completed in June 2016.[1,2] The Materials Chemistry lab at the School of Chemistry, University of Nottingham subsequently obtained a short length (~2 feet) of a heavily charred wooden beam (Figure S1 and S2) so as to explore the properties of such a uniquely formed material. The heat of the fire caused the carbonisation of the wood into carbon and as such the resulting carbonaceous material will be referred to as air-carbonized wood.

Activated carbons may be generated from various forms of carbonaceous matter. Amongst the processes used to generate activated carbons, KOH has been studied as an activating agent to develop porosity in a range of precursor carbonaceous materials since the late 1970s.[3] Carbon precursors that have been studied include non-porous carbons derived from various forms of biomass, such as rice husks, coconut-shells, wood, sawdust, and fruit stones.[4-14] Activated carbons from non-biomass derived carbonaceous materials, such as anthracite, coke, lignite, and other forms of coal have also been studied.[15-18] KOH has also been used successfully to improve and modify the porosity of already porous carbon materials such as zeolite-templated carbons (ZTCs), and carbide-derived carbons (CDCs),[19-21] or structured carbon materials such as carbon nanotubes, and graphene.[22,23] However, carbonaceous matter formed from the burning of biomass in air has never, to the best of our knowledge, been studied as precursor for the production of activated carbon. Thus in obtaining a sample of burnt-wood from the CNL site we gave ourselves an opportunity to explore, for the first time, the production of activated carbon from what may be regarded as air-carbonized wood. This is particularly interesting since the nature of the carbon feedstock has a significant impact on porosity development in activated carbons derived from various sources.[24-30]

This work is also a departure from known practice given that although activated carbons can be produced using biomass feedstock, the biomass is first carbonized, usually via thermal decomposition of carbonaceous matter into an essentially all-carbon material. The carbonisation process is usually performed by heat treatment (400 – 900 ºC) under a non-oxidising (e.g. nitrogen or argon) atmosphere.[9,10,12,13,30,31] After evolution of volatiles, the remaining carbon atoms reorganise into aromatic rings forming graphitic micro-crystallites, but with no long-range graphite structure.[13] Studies into the carbonization of lignocellulosic materials have found the main decomposition processes (involving evolution/release of $H_2O$, $CO_x$, $CH_4$, and light hydrocarbons) to occur in the temperature range of 200 – 350 ºC. Little weight loss is observed above 500 ºC implying that the main structural changes are completed by this temperature.[32,33] An alternative biomass carbonisation route is via heating of organic or biomass precursors dispersed in water at relatively low temperatures (220 – 250 ºC) to generate so-called hydrothermal chars.[14,34-36] Although complete carbonization of biomass via burning in air under ambient pressure conditions has not been studied, the effect of heat treatment of cellulose (as rayon) in the presence of oxygen, prior to a carbonization step under nitrogen has been explored.[37] Pastor *et al.*[37] studied the effect of oxidation of biomass in O/He (1:4) flow at 230 – 250 ºC, prior to carbonization in $N_2$/He (1:4) flow at 850 ºC and found that pre-oxidation caused an increase in carbon yield (24% vs. 18% without pre-oxidation) due to the oxidation of cellulose hydroxyl groups to carboxyl groups. This bypassed the production of levoglucosan from cellulose, which decomposes easily and reduces carbon yield. The formation of H-bonds between carboxyl groups offers some stability during further heat treatment.[38] Thus carbon residues may be obtained via thermal treatment of biomass under air or reduced air conditions.

Many applications of porous carbons require careful control over the nature of the porosity of the carbon. For example, use of carbons as electrode materials in supercapacitors requires the formation of pores suitable for the particular electrolyte used.[24,39,40] Porous carbons

have also been studied as potential hydrogen storage materials, where pores with widths of ~ 6 Å have been found to be optimum for $H_2$ uptake.[41-45] Thus, it is clear that careful control of pore size is very importance when targeting porous carbons for specific applications. A potentially major application of porous carbons that requires careful control of porosity is $CO_2$ capture and storage (CCS). $CO_2$ is the major greenhouse gas, and is responsible for a significant part of the so-called greenhouse effect.[46] Production of $CO_2$ can be decreased by either transitioning from fossil-fuel power stations to generating energy from renewable sources, or by decreasing energy consumption through increased energy efficiency. These options are the end goals in terms of reduction of $CO_2$ emissions and halting greenhouse effects, but before they are achieved a mid-term solution exists in the form of $CO_2$ capture and sequestration.[47] Current industrial $CO_2$ adsorption processes use monoethanolamine (MEA) solution to capture $CO_2$ from flue gas streams via the formation of MEA carbamate in a process known as 'aqueous amine scrubbing'. Although this method can be applied on an industrial scale, there are a number of shortcomings, namely, (i) MEA is toxic and causes corrosion of equipment, (ii) affinity of MEA for other species ($SO_2$, $NO_2$, HCl, HF, $O_2$) in the flue gas stream causes degradation of the amine, and (iii) heating of the MEA carbamate solution to evolve pure $CO_2$ and recycle the MEA is an inefficient high energy consumption process. Furthermore, MEA systems have low $CO_2$ loading capacity.[48] An alternative $CO_2$ capture route is via the use of porous solid phase adsorbents,[49,50] wherein activated carbons are particularly suited due to their controllable porosity, low cost, and chemical stability.[24,51-53]

This work provides a first account of the porosity generated in air-carbonized wood as a function of the activation conditions with KOH concentration, temperature of activation, and pre-activation compaction as the variables. Furthermore, given the nature of the porosity generated in the activated CNL1 carbons, we also explore their $CO_2$ uptake properties as a likely end use.

## 2. Experimental Section

### 2.1 Materials

The nature of the starting material (referred to as 'CNL1 carbon') meant that no carbonization step was required prior to activation. A small amount of CNL1 carbon (~25 g) was taken from the surface of the burnt wood (Figure S1), and used as starting material for activation. Interestingly, a cross-section of the charred beam revealed the inner core of the wood to be relatively intact (Figure S2) and thus for uniformity and repeatability the CNL1 carbon was harvested from fully carbonaceous matter on the surface of the beams. The carbon was ground into a fine powder and thoroughly mixed with KOH at KOH/CNL1 weight ratio of 2 or 4. The KOH/CNL1 mixture was then heated either as a powder (conventional activation) or as a pellet (compactivation) formed by compaction of the powder mixture at 740 MPa. Typically, 5 g KOH/CNL1 mixture was prepared with half conventionally activated as powder and the other half compactivated in the form of pellets. The KOH/CNL1 powder or pellet was heated to the target temperature (600 - 800 $^{o}$C) in a horizontal tube furnace under nitrogen atmosphere. A heating ramp rate of 5 $^{o}$C min$^{-1}$ was used, and samples were held at the target temperature for 1 h before cooling to room temperature whilst still under a flow of nitrogen. The resulting activated or compactivated carbon was washed in 2M HCl at room temperature overnight to remove any inorganic residues, followed by multiple washing with deionized water until neutral pH was achieved. Finally the carbons were dried in air at 120 $^{o}$C. The activated carbons were designated as CNL1-xT, where x is the KOH/CNL1 carbon ratio (i.e., 2 or 4), and T is temperature of activation (600, 700 or 800 $^{o}$C). Compactivated carbons were labelled in a similar manner but denoted with 'P'. For example, a conventionally activated powder form of activated carbon prepared at KOH/CNL1 ratio of 4 and 800 $^{o}$C is designated as 'CNL1-4800', while a sample compactivated as pellet at KOH/CNL1 ratio of 2 and 600 $^{o}$C is designated as 'CNL1-2600P'.

### 2.2 Characterisation of samples

Thermogravimetric analysis (TGA) was performed using a TA Instruments SDT Q600 analyser under flowing air conditions (100 mL/min). Powder XRD analysis was performed using a PANalytical X'Pert PRO diffractometer with Cu-Kα light source (40 kV, 40 mA) with step size of 0.02° and 50 s time step. CHN elemental analysis was performed using an Exeter Analytical CE-440 Elemental Analyser. Analysis of porosity and determination of textural properties was performed via nitrogen sorption using a Micromeritics ASAP 2020 sorptometer. Prior to analysis (at -196 °C), the carbon samples were degassed under vacuum at 200 °C for 12 h. Surface area was calculated using the Brunauer-Emmett-Teller (BET) method applied to adsorption data in the relative pressure ($P/P_o$) range 0.02 – 0.22. The total pore volume was determined from the total nitrogen uptake at close to saturation pressure ($P/P_o \approx 0.99$). The micropore surface area and micropore volume were determined via *t*-plot analysis. Non-local density functional theory (NL-DFT) was applied to nitrogen adsorption isotherms to determine the pore size distribution. SEM images were recorded using an FEI Quanta200 microscope, operating with a 5 kV accelerating voltage. Transmission electron microscopy (TEM) images were obtained using a JEOL 2100F instrument operating at 200 kV equipped with a Gatan Orius CCD for imaging. The samples were suspended in distilled water and dispersed onto lacey carbon support film prior to analysis.

### 2.3 $CO_2$ uptake measurements

$CO_2$ uptake was determined using a Hiden Isochema Intelligent Gravimetric Analyser (IGA-003). Before $CO_2$ uptake measurements, the carbon samples were degassed at 200 °C under vacuum for several hours. Adsorption-desorption isotherms were measured at 25 °C over $CO_2$ pressure range of 0 – 20 bar.

## 3. Results and Discussion

### 3.1 Confirmation of carbonization and nature of CNL1 carbon

Prior to activation of the CNL1 carbon, it was necessary to confirm that it was fully carbonaceous. This assessment was carried out using TGA, powder XRD, and elemental (CHN) analysis. Figure 1 shows the TGA curve for the raw CNL1 carbon under heat treatment to 1000 $^{o}$C at 10 $^{o}$C min$^{-1}$ in flowing air. The CNL1 carbon is stable below 300 $^{o}$C, after which combustion is observed as a single step mass-loss event between 300 and 480 $^{o}$C. All of the raw CNL1 carbon was completely burnt off with virtually no residue left at 800 $^{o}$C, which confirmed a fully carbonaceous nature. If a significant amount of non-carbonized wood (e.g., lignocellulosic matter) had been present, the mass loss due to burn-off would not have occurred in a single event, as the main components of wood (lignin, cellulose, and hemicellulose) decompose at different temperatures.[54] The absence of a mass loss event below 200 $^{o}$C indicates that the CNL1 carbon contains no residual water and is therefore likely to be highly hydrophobic. The single step burn-off implies uniformity of the carbonaceous matter, whilst the rather broad combustion temperature range (300 – 480 $^{o}$C) points to an amorphous carbon structure, as significant crystallinity would show a more discrete burn due to cooperative melting effects. Powder XRD analysis of the CNL1 carbon (Figure S3) reveals two broad peaks centred at 2-theta of ~22$^{o}$, and ~44$^{o}$. These peaks are diffractions from (002), and (100) planes of graphitic carbon, respectively, which may suggest the presence of graphitic domains. However, the broad nature of the peaks indicates that any graphitic domains do not have any significant planarity as the carbon is predominantly amorphous in nature.

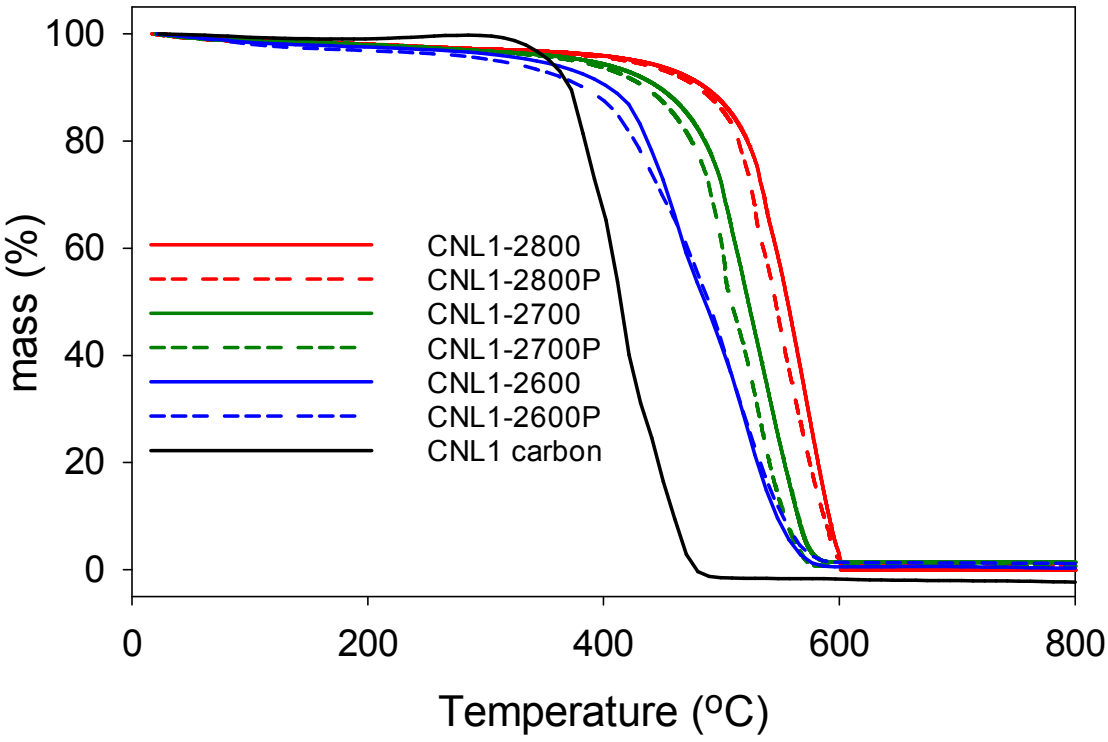


**Figure 1**. Thermogravimetric analysis (TGA) curve of CNL1 carbon and activated CNL1-2T carbons thermally treated in air.

The elemental C, H and O content for the raw CNL1 carbon is generally comparable to that of other biomass-derived chars (Table S1). However, it is noticeable that the elemental C content of the CNL1 carbon is relatively high, especially when compared to biochars (so-called hydrochars) obtained via hydrothermal carbonisation (Table S1). Moreover, whilst the N content of biochars is generally ~ 5 %, total removal of N appears to have occurred during burning of the CNL1 wood. Based on SEM images (Figure 2 and Figure S4), the morphology of the CNL1 carbon is typical of chars formed from lignocellulosic biomass, and is similar to that previously observed by Wu *et. al*.[9,10] An extended honeycomb structure can be clearly seen, showing retention of the pre-carbonization structure of wood. The CNL1 carbon is lowly porous (Figure S5) with surface area of 100 $m^2$ $g^{-1}$ and pore volume of 0.06 $cm^3$ $g^{-1}$, micropore surface area of 79 $m^2$ $g^{-1}$ and micropore volume of 0.035 $cm^3$ $g^{-1}$. The pore size distribution curve of CNL1

carbon (Figure S5) suggest the presence of pores of size 7 Å and 12 Å, which can also be visualised on TEM images (Figure S6). The CNL1 carbon is therefore somewhat more porous than other biomass-derived biochars obtained via pyrolysis under inert conditions or via hydrothermal carbonisation.[24]

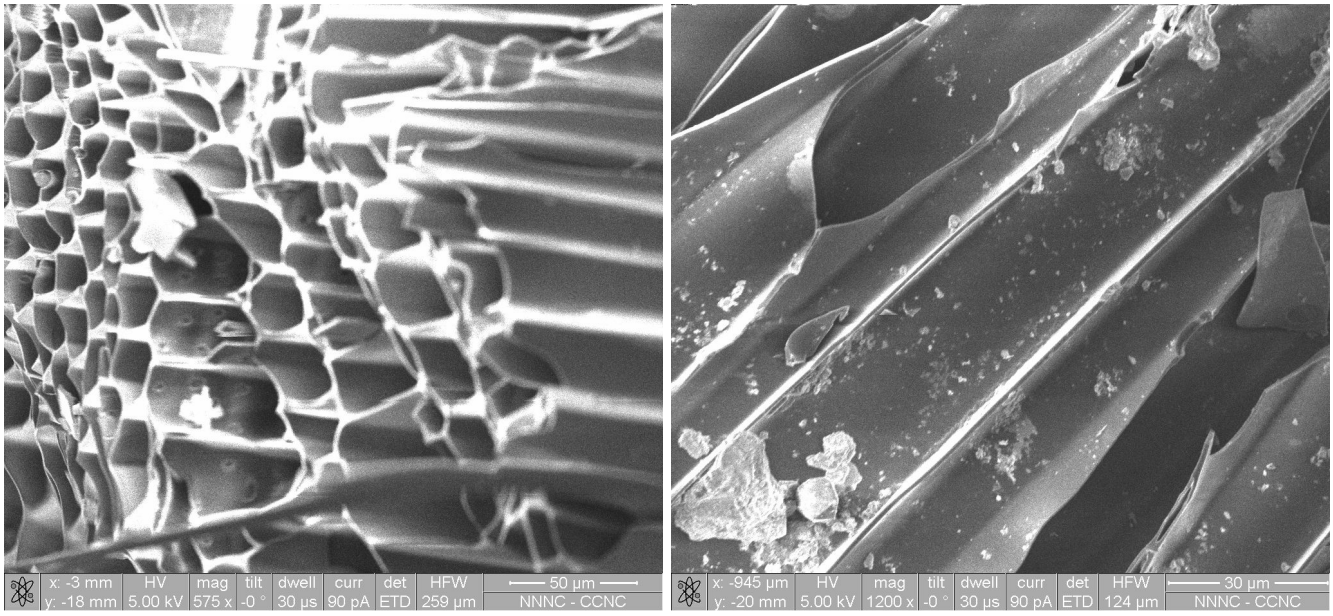


**Figure 2**. SEM images of CNL1 carbon.

### 3.2 Yield and properties of activated CNL1 carbons

The yield of activated carbons is an important consideration in the evaluation of new types of raw materials. The typical yield of activated carbons with moderate to high porosity is 15 – 40 wt%.[24,55-57] As far as we can tell from available literature data, the highest yield reported so far for KOH activation is ca. 40 wt%, which occurs at the lowest levels of activation.[24,55-57] It is therefore highly noteworthy, as shown in Table 1, that the activation of CNL1 carbon generates much higher yields of activated carbon in the range of 30 – 80 wt%. The yield is greatest (80 wt%) under the mildest conditions (KOH/CNL1 carbon ratio of 2 at 600 ºC) and least (32 wt%) at the severest activation regime (KOH/CNL1 carbon ratio of 4 at 800 ºC). Such high yields of

activated carbon, under the prevailing activation conditions, have hitherto not been observed. Indeed, at all levels of activation, the yields of activated CNL1 carbons are twice as high as those previously reported for precursors such as biochar or polypyrrole (Table S2).[55-57] Thus the CNL1 carbon may be described as being resistant towards activation. Compactivation has no clear trend on the yield as there is a mix of values with yields for compactivated samples being higher, lower, or identical to conventionally activated analogues. As shown in Figure 1 (and Figure S7) all the activated CNL1 carbons show relatively high thermal stability, which is higher than that of the raw CNL1 carbon. The activated carbons are burnt off (residual mass typically below 1 wt%) in a single mass-loss event between 300 and 600 ºC. In all cases, the activated CNL1 carbons show virtually no mass loss below 200 ºC, which suggests that, similar to the raw CNL1 carbon, they have hardly any adsorbed water. A noteworthy observation is that the thermal stability of the carbons increases as the activation temperature rises. Thus, the temperature of maximum burn-off rises from 485 ºC for CNL1-2600 to ca. 520 and 555 ºC, respectively, for activation at 700 (CNL1-2700 and CNL1-2700P) and 800 ºC (CNL1-2800 and CNL1-2800P). A similar trend is observed for carbons activated at KOH/ratio of 4 (Figure S7). In general, compactivated carbons burn off at a slightly lower temperature compared to their conventionally activated analogues. Mass losses due to burn-off become more discrete for more severely activated samples in a manner similar to that observed by Song *et. al.*,[13] where thermal stability of KOH-activated carbons derived from poplar anthers increased from 500 to 590 ºC as activation temperature rose from 500 to 800 ºC. The effect of activation temperature in raising thermal stability may be related to the formation of graphitic domains that are favored by exposure to heat treatment at elevated temperature.

**Table 1**. Yield, textural properties and $CO_2$ uptake of activated CNL1 carbons.

| Sample | Yield[a] (wt%) | Surface area[b] ($m^2$ $g^{-1}$) | Pore volume[c] ($cm^3$ $g^{-1}$) | Pore size[d] (Å) | $CO_2$ uptake[e] (mmol $g^{-1}$) | | |
|---|---|---|---|---|---|---|---|
| | | | | | 0.15 bar | 1 bar | 20 bar |
| CNL1 carbon | | 100 (79) | 0.06 (0.035) | 7/12 | | | |
| CNL1-2600 | 80 | 1190 (1107) | 0.55 (0.49) | 5.5/7/9 | 1.2 | 3.5 | 8.4 |
| CNL1-2600P | 81 | 1281 (1179) | 0.61 (0.52) | 5.5/7/9 | 1.3 | 3.8 | 9.1 |
| CNL1-2700 | 65 | 1399 (1343) | 0.63 (0.59) | 6/8.5/12 | 1.3 | 4.8 | 13.4 |
| CNL1-2700P | 66 | 1554 (1486) | 0.70 (0.65) | 6/8.5/12 | 1.4 | 5.0 | 14.8 |
| CNL1-2800 | 52 | 1326 (1263) | 0.60 (0.55) | 6/8.5/13 | 1.0 | 4.3 | 14.1 |
| CNL1-2800P | 76 | 1795 (1722) | 0.89 (0.75) | 7/8.5/13 | 1.1 | 4.5 | 16.4 |
| CNL1-4600 | 68 | 1121 (1021) | 0.53 (0.45) | 6/8.5/12 | 1.0 | 3.0 | 9.5 |
| CNL1-4600P | 58 | 1881 (1723) | 0.89 (0.76) | 5.5/8.5/12 | 1.0 | 3.9 | 15.5 |
| CNL1-4700 | 53 | 1280 (1191) | 0.65 (0.56) | 6.5/8.5/15 | 1.0 | 3.3 | 10.5 |
| CNL1-4700P | 56 | 2315 (2158) | 1.08 (0.96) | 7/8.5/15 | 0.9 | 4.0 | 20.3 |
| CNL1-4800 | 32 | 2183 (1886) | 1.05 (0.84) | 6.5/8.5/16 | 0.8 | 3.3 | 14.5 |
| CNL1-4800P | 49 | 2487 (2296) | 1.16 (1.01) | 6.5/8.5/16 | 0.8 | 3.7 | 19.4 |

[a]The yield is based on starting weight of CNL1 carbon. The values in the parenthesis refer to: [b]micropore surface area and [c]micropore volume. [d]Pore size distribution maxima obtained from NLDFT analysis. [e]$CO_2$ uptake at 25 $^oC$ and various pressures (i.e., 0.15 bar, 1 bar and 20 bar).

The XRD patterns of the activated carbons (Figure S8) are similar to that of the CNL1 carbon in the 2-theta range of 5 – 80$^o$, and show two broad peaks centred on 2θ = 22$^o$ and 44$^o$, which are diffractions of the (002), and (100) planes of poorly ordered graphitic domains, respectively. In agreement with the TGA curves (Figure 1 and Figure S7), it is clear that the XRD patterns of activated carbons prepared at higher temperature show better defined 'graphitic' peaks, implying greater graphitisation, which would engender higher thermal stability. This is most noticeable for the peak at ~44$^o$, whilst the peak at ~22$^o$ becomes obscured by distortions of the baseline.[58,59] CHN analysis of a representative activated carbon (CNL1-4800) indicated a significant increase in elemental carbon content to 91 wt% (compared to 77.7

wt% for the raw CNL1 carbon – Table S1). The H content decreases significantly to < 0.3 wt% (from 3.2%), while the amount of O reduces to 9.3 wt% (from 19.1 wt%). The activation process, therefore, yields highly carbonaceous materials with much reduced H and O containing groups.

Porosity studies are crucial given the surprisingly high yield of the activated CNL1 carbons and the fact that significant activation (i.e. creation of high levels of porosity) relies on carbon etching. The nitrogen sorption isotherms obtained for activated CNL1 carbons prepared at KOH/CNL1 carbon ratio of 2 are given in Figure 3A. All the activated and compactivated CNL1-2T carbons exhibit type I isotherms that are typical of microporous materials.[60] The isotherms confirm that despite the high yields, the CNL1-2T carbons are highly porous. It is noteworthy that activation temperature in the range 600 – 800 $^{o}$C has very little effect on the nature (i.e., shape) of the isotherm. This is surprising because most previous studies have noted a widening of the adsorption knee at higher activation temperature.[29,56,57,61-74] The level of porosity generated, as judged by the amount of nitrogen adsorbed, increases modestly for samples prepared at higher activation temperature despite the non-changing nature and shape of the isotherms. The isotherms of the compactivated carbons are similar to those of analogous conventionally activated carbons except that they exhibit higher amounts of nitrogen sorption. Thus in all cases compactivation generates higher levels of porosity, which is consistent with previous studies.[56,73]

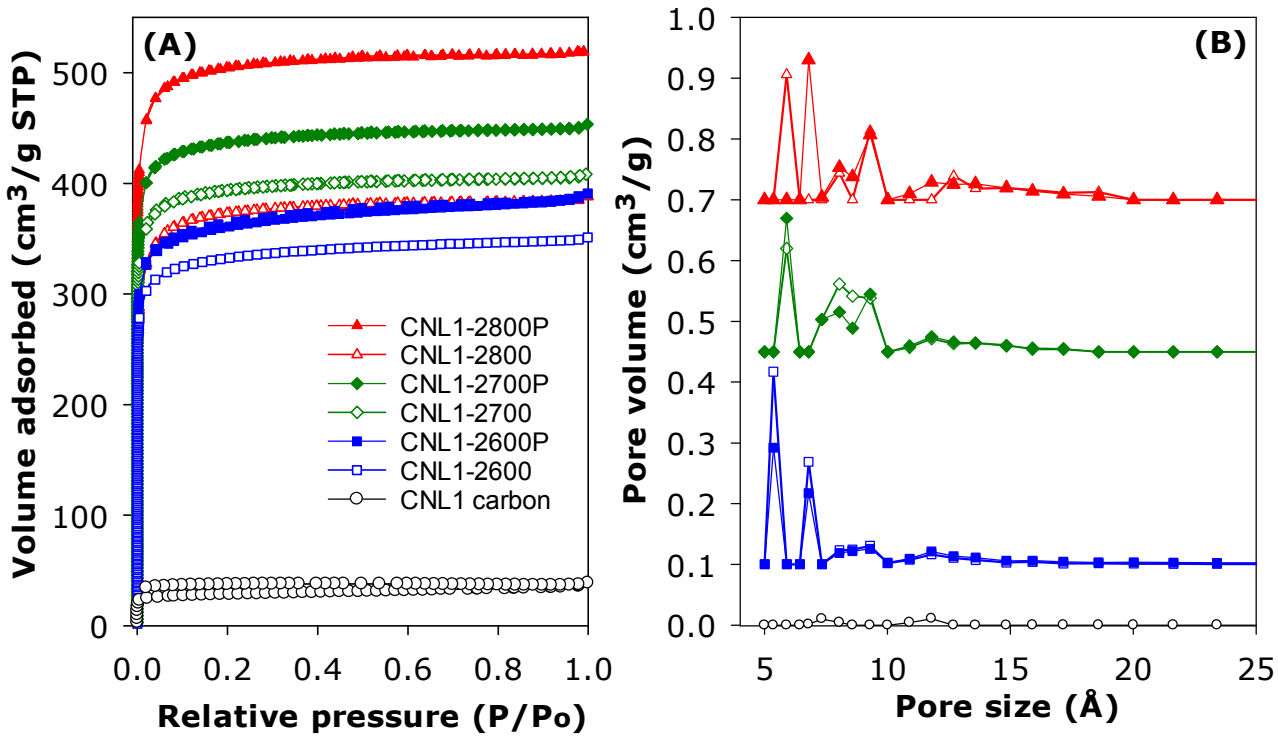


**Figure 3**. (A) Nitrogen sorption isotherms and (B) pore size distribution curves of activated and compactivated carbons derived from CNL1 carbon activated at 600 – 800 ºC and KOH/carbon ratio of 2.

The similarity in nature of the isotherms is related to the size of pore channels present in the activated carbons as shown by the pore size distribution curves in Figure 3B, which confirm that all the CNL1-2T samples mainly possess micropores. The main pore size maxima values, summarized in Table 1, show that the porosity of the CNL1-2T samples is dominated by small micropores and that there are hardly any pores larger than 10 Å and virtually no pores larger than 15 Å. The samples possess micropores with the smallest pores centered at 5 - 7 Å, medium pores at ca. 8.5 Å and a minor proportion of larger pores in the range 12 – 13 Å. The size of pores (or pore size distribution) is identical for conventionally activated and compactivated carbons (Figure 3B and Table 1), which confirms that the higher porosity of the compactivated carbons is not accompanied by pore enlargement.[56,73]

The nitrogen sorption isotherms obtained for activated CNL1-4T carbons prepared at KOH/CNL1 carbon ratio of 4 are shown in Figure 4A. Despite the increase in amount of KOH used, the resulting CNL1-4T samples exhibit isotherms that are still remarkable typical of microporous materials. Furthermore, increase in activation temperature from 600 to 800 $^{o}$C, whilst resulting in an increase in the amount of nitrogen adsorbed, does not significantly alter the isotherm shape. Thus even CNLI-4T samples prepared under the severest conditions (KOH/CNL1 carbon ratio of 4 at 800 $^{o}$C) are still highly microporous as witness the pore size distribution curves in Figure 4B wherein the porosity is dominated by pores centered at 5 - 7 Å for the smallest pores, 8.5 Å for medium pores and 15 – 16 Å for the largest pores. Indeed, it is remarkable that there are hardly any pores larger than 20 Å. In all cases, compactivation, generates higher levels of porosity but with no significant change in the size of pore channels.

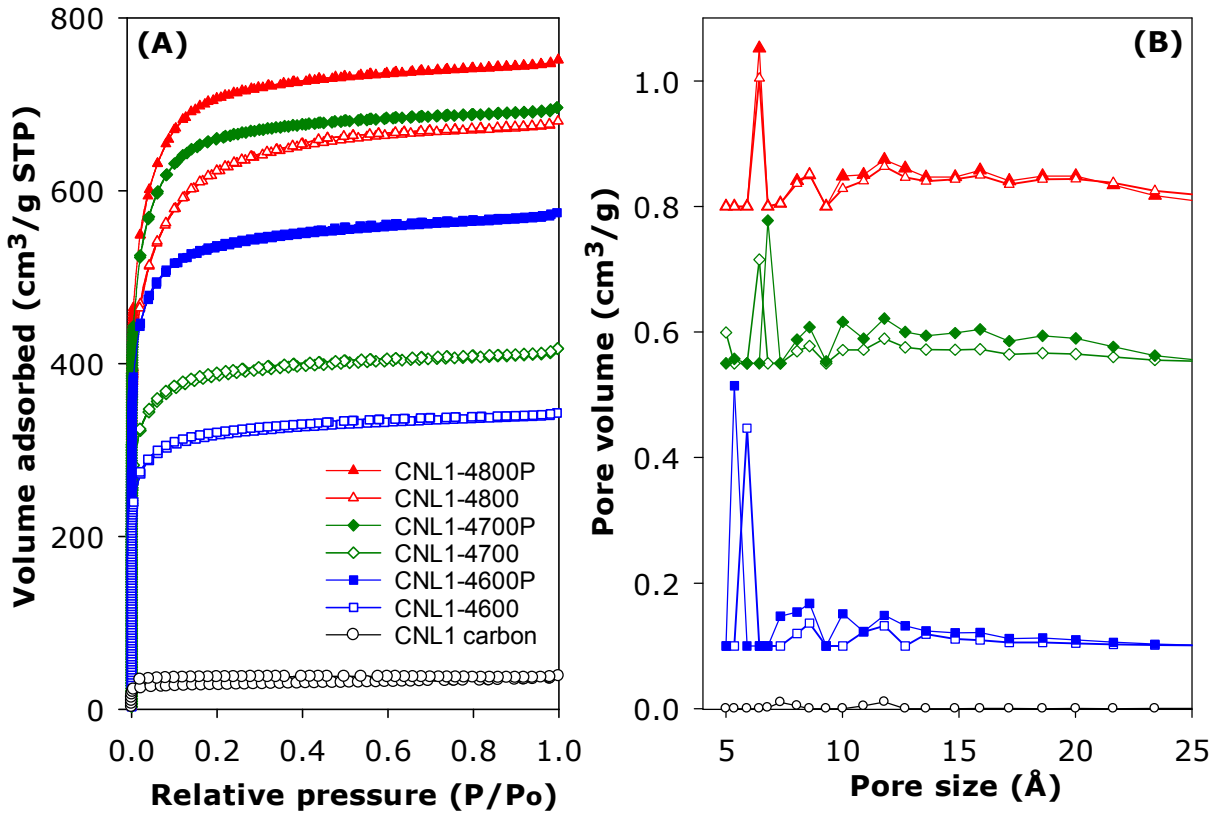


**Figure 4**. (A) Nitrogen sorption isotherms and (B) pore size distribution curves of activated and compactivated carbons derived from CNL1 carbon activated at 600 – 800 $^{o}$C and KOH/carbon ratio of 4.

The textural properties of conventionally activated and compactivated CNL1-xT carbons are summarized in Table 1. The carbons have moderate to high surface area; for CNL1-2T samples, the surface area is within the narrow range of 1190 – 1326 $m^2$ $g^{-1}$ for conventionally activated carbons and 1281 – 1795 $m^2$ $g^{-1}$ for compactivated carbons. The total pore volume also varies within narrow ranges of 0.55 – 0.63 $cm^3$ $g^{-1}$ for activated carbons and 0.61 – 0.89 $cm^3$ $g^{-1}$ for compactivated carbons. The modest increase in the textural properties at higher activation temperature is consistent with the resistant nature of the CNL1 carbon with respect to activation. Furthermore, compactivation only causes a modest rise in the textural properties especially at 600 and 700 ºC, where the increase is only 10% but reaches ca. 40% at 800 ºC. It is noteworthy that the proportion of surface area and pore volume arising from micropores is very high for the CNL1-2T samples, being typically ~ 95% for surface area and ~ 92% for pore volume. For the CNL1-4T samples, the surface area of activated carbons varies from 1121 and 1289 $m^2$ $g^{-1}$ at 600 and 700 ºC, respectively, to 2183 $m^2$ $g^{-1}$ at 800 ºC, while for compactivated carbons it is 1881 $m^2$ $g^{-1}$ (600 ºC), 2315 $m^2$ $g^{-1}$ (700 ºC) and 2487 $m^2$ $g^{-1}$ at 800 ºC. Thus it is only under the severest activation conditions (i.e., at 800 ºC) that surface area above 2000 $m^2$ $g^{-1}$ is observed for conventionally activated CNL1-4T carbons, while for compactivated sample it is achieved at 700 ºC.[56,73] The pore volume follows a similar trend with values above 1 $cm^3$ $g^{-1}$ observed for both activated and compactivated CNL1-4T samples only at 800 ºC. Similar to the CNL1-2T series, it is clear that CNL1-4T samples achieve a lower level of textural properties compared to carbons from other types of precursors, which we ascribe to the resistant nature of the CNL1 carbon with respect to activation. It is especially noteworthy that the proportion of surface area and pore volume arising from micropores remains typically above 85% at 600 and 700 ºC, and is still remarkably high (i.e., 50%) even after activation at 800 ºC.

The porosity data in Figure 3, Figure 4, and Table 1 confirm that the air carbonized CNL1 carbon is resistant with respect to activation and is therefore an excellent precursor for the formation of highly microporous activated carbons. Regarding hard to activate biomass-derived carbonaceous matter, it is generally accepted that lignin-derived biochar (generated via pyrolysis under inert conditions or hydrothermal carbonisation) is one of the more difficult precursors to activate.[57,75-77] We therefore compared the nitrogen sorption isotherms and pore size distribution of the activated CNL1 carbons with lignin-derived activated carbons[57] prepared at 800 ºC and KOH/carbon ratio of 2 (Figure S9) or ratio of 4 (Figure S10), along with other carbons derived from grass,[74] carbon nanotube superstructures[61] or polypyrrole.[55,56] It is clear from the comparison (Figure S9, Figure S10 and Table S3) that the retention of microporosity is far higher in the activated CNL1 carbons compared to the other four previously reported classes of carbons. Even when activated at KOH/carbon ratio of 4 at 800 ºC, the resulting CNL1-4800 sample is still predominantly microporous compared to all the other analogous samples that are mesoporous (Figure S10 and Table S3). This comparison presents intriguing questions about the nature of the CNL1 carbon. It has previously been postulated that lignin derived biochars are difficult to activate due to their high lignin content (compared to cellulose) and also due to the highly cross-linked in nature of lignin biochars.[75-77] It is therefore likely that during the burning of wood that generated the CNL1 carbon, the proportion of lignin products compared to cellulose products may have been enhanced due to easier burning of the later. Several studies have already established that lignin is thermally more stable in air compared to cellulose,[78,79] which is consistent with enrichment of the former in the CNL1 carbon. Clearly, the activation of the CNL1 carbon favors formation of micropores, which in turn limits the total surface area and pore volume that can be reached. A comparison of all the CNL1-xT carbons with analogous activated carbons (Table S4, Figure S11 and Figure S12) establishes the 'resistant' nature of the CNL1 carbon and which favors

the formation of micropores event at the severest activation conditions. Indeed, whilst sample CNL1-4800 and CNL1-4800P are predominantly microporous, analogous samples from lignin, grass, CNT composites and polypyrrole are mesoporous (Figure S10). Furthermore, for CNL1-xT carbons, the activation temperature has a far lower effect on the level of surface area and pore volume achieved (Figure S11 and Figure S12).

To confirm that the resistant to activation nature of the CNL1 carbon was due to the manner in which the biomass (wood) was converted to carbonaceous matter, we pyrolysed wood chippings (Figure S2) under nitrogen and then activated the resulting carbon to yield activated carbons (designated as CNLW-xT, where x is KOH/carbon ratio and T is activation temperature). We then compared the yield and porosity of the samples derived from 'nitrogen carbonized' wood to similarly activated samples derived from 'air-carbonized' wood, i.e., the CNL1 carbon (Table S5). This comparison revealed that activated carbon from nitrogen carbonized wood has lower yield, higher surface area and larger pores, which all suggest lower resistance to activation compared to the air-carbonized CNL1 carbon. When we carbonized wood via hydrothermal carbonization, activation of the resulting hydrochar yielded activated carbons with properties similar to CNLW-xT samples. The comparative data (Table S5) is very revealing with clear trends whereby the yields of the 'air-carbonized' samples are higher, but the textural properties are lower and with greater microporosity. These comparisons suggest that the key to the resistance of the air carbonized CNL1 carbon to activation is a likely enrichment of lignin-derived carbon content and that such enrichment is favored under carbonization in the presence of limited air. To explore this proposition further, we carbonized biomass (wood chippings) under lab conditions that allowed some ignition (see Supporting information for lab-based air carbonization procedure). The biomass (wood chippings) was converted to carbon (Supporting Figure S13) with a yield of 20 – 30 wt% depending on the carbonization temperature. The thermal stability of the lab prepared

air-carbonized sample was very similar to that of the CNL1 carbon and in any case higher than that of carbon pyrolysed under nitrogen (Supporting Figure S14). The CNL1 carbon and lab air-carbonized sample burn off between 315 and 480 ºC, while the lab $N_2$-carbonized sample is less thermally stable and burns off between 250 and 375 ºC. As discussed above, the higher thermal stability of the air-carbonized samples is due to enrichment of lignin-derived carbonaceous matter.[54] Furthermore, the XRD patterns of the lab prepared air-carbonized carbons were virtually identical to that of the CNL1 carbon (Supporting Figure S15). The similarity between the lab air carbonized samples and CNL1 carbon was also confirmed by porosity analysis (Supporting Figure S16 and Table S6). The nitrogen sorption isotherms and pore size distribution of lab air carbonized sample are similar to those of the CNL1 carbon (Supporting Figure S16). The textural properties (Surface area, pore volume and microporosity) of the lab generated air-carbonized sample are similar to those of CNL1 carbon (Table S6).

Thus the lab prepared air-carbonized carbonaceous matter is similar in nature to the CNL1 carbon. Our findings on the effects of combustion of biomass on the properties of resulting carbonaceous matter are consistent with previous reports.[75-81] Furthermore, previous reports have shown that it is possible to generate high carbon yields by performing so-called flash carbonization of biomass under pressurized air conditions that allow some ignition of the biomass.[82] Overall, it is therefore possible to prepare CNL1 type carbon in the lab, which makes such carbon a viable route for the synthesis of activated carbons with the interesting properties described above. Although outside the scope of this work, we note that activated carbon generated from the lab air carbonized carbonaceous matter is similar to activated CNL1 carbon in terms of having high yield, high density and high microporosity.

### 3.3 Gravimetric $CO_2$ uptake of activated CNL1 carbons

Given the highly microporous nature of the activated CNL1 carbons, we probed their capacity for $CO_2$ capture and storage at room temperature (25 $^oC$) and pressure range of 0 to 20 bar. The $CO_2$ uptake isotherms for CNL1-2T carbons are shown in Figure 5 (and supporting Figure S17) and the storage capacity at various pressures (0.15, 1 and 20 bar) is stated in Table 1. Most studies that are aimed at exploring the post-combustion capture of $CO_2$ generally emphasize the uptake at 1 bar; for CNL1-2T carbons the storage capacity at 1 bar ranges between 3.5 mmol $g^{-1}$ for sample CNL1-2600 to a high of 5.0 mmol $g^{-1}$ for CNL1-2700P. The CNL1-2T carbons, therefore, show a very high gravimetric $CO_2$ uptake that is one of the highest ever reported for porous carbons.[14,29,56,72-74,83-88] In all cases, compactivated carbons have higher $CO_2$ uptake than their activated analogues,[56,73] with sample CNL1-2700P having the highest uptake. Given that post-combustion flue gas streams from power stations will typically consist of ca. 15% $CO_2$ with the remainder being mainly $N_2$ (70–75%), and water (5–7%),[89,90] it is necessary to consider the $CO_2$ uptake at 0.15 bar. The $CO_2$ uptake at 0.15 bar is within the impressive range of 1.0 to and 1.4 mmol $g^{-1}$ (Table 1 and supporting Figure S17). In all cases compactivation improves the uptake capacity, and the best $CO_2$ absorbing sample is achieved via activation or compactivation at 700 $^oC$. In general the uptake at 0.15 and 1 bar shows no clear correlation with the surface area and pore volume of the samples. However, the narrow range of the $CO_2$ uptake at these low pressures is a reflection of the similar pore size of the CNL1-2T samples as discussed above. This observation once again emphasises the importance of pore size in determining the low pressure (< 1 bar) $CO_2$ uptake of porous carbons under ambient conditions.[14,29,51,56,57,61] On the other hand, at 20 bar, the $CO_2$ uptake generally rises for samples with high surface area, which means that compactivation and a high activation temperature enhance the storage capacity; at 20 bar the lowest uptake is for sample CNL1-2600 (8.4 mmol $g^{-1}$) and highest for

CNL1-2800P (16.4 mmol $g^{-1}$). Overall, though, the gravimetric $CO_2$ uptake of the CNL1-2T carbons at 0.15 and 1 bar is certainly impressive and shows the potential of these air-carbonized wood-derived carbons as post-combustion $CO_2$ storage materials.

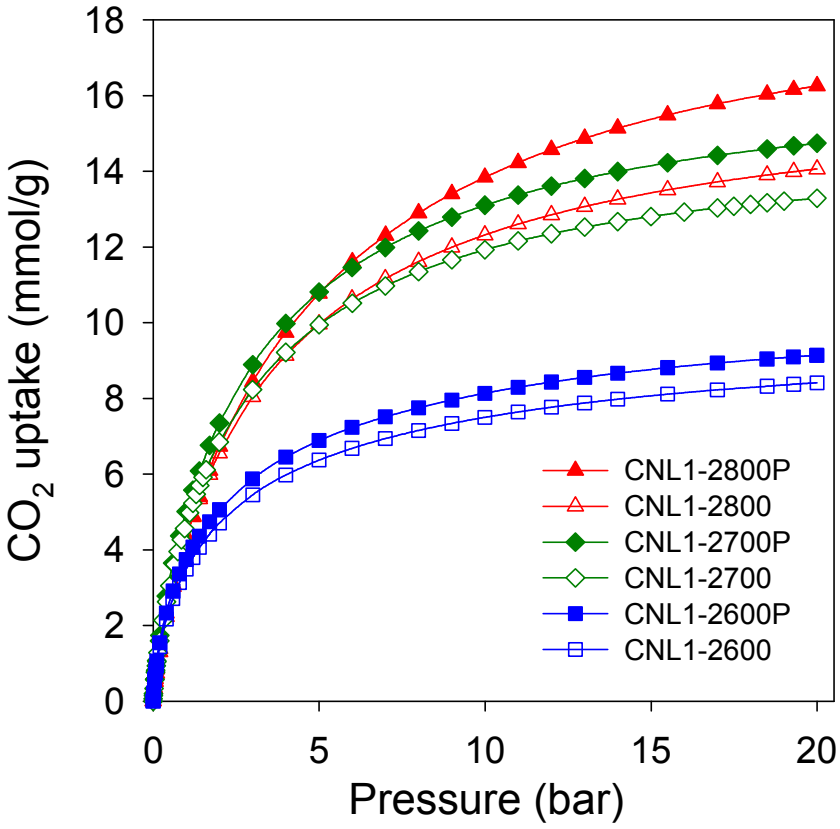


**Figure 5**. $CO_2$ uptake isotherms at 25 ºC and 0 - 20 bar for activated CNL1-2T carbons.

Assessment of porosity data discussed above suggests that, compared to CNL1-2T samples, the CNL1-4T set of carbons should exhibit higher $CO_2$ uptake at 20 bar but lower uptake at pressure of 1 bar or lower. This is indeed what is observed as shown in Figure 6 (and supporting Figure S18) and Table 1. The uptake at 0.15 bar ranges between 0.8 and 1.0 mmol $g^{-1}$ and generally decreases, if only slightly, as pore size of samples increases at higher activation temperature. For CNL1-4T samples, compactivation has little effect of the $CO_2$

uptake at 0.15 bar. At 1 bar, the $CO_2$ uptake varies between 3.0 and 4.0 mmol $g^{-1}$, and in all cases compactivation offers significant rises in uptake compared to conventional activation. As expected, the CNL1-4T carbons with the highest surface area show impressive $CO_2$ uptake of up to 20.3 mmol $g^{-1}$ at 20 bar. The $CO_2$ uptake, at 20 bar, closely matches the trend in surface area, and thus compactivation causes drastic enhancement in uptake of 63% at 600 $^oC$, 93% at 700 $^oC$ and 33% at 800 $^oC$ (Table 1). Unusually though, sample CNL1-4700P and CNL1-4800P exhibit attractive $CO_2$ uptake under both low and high pressure conditions. This is a departure from the usual trend wherein carbons that exhibit high uptake at 20 bar tend to have much lower storage capacity at pressure $\leq$ 1 bar. This trend is usually caused by the fact that in most porous carbons, narrow pore channels (suitable for low pressure uptake) are not accompanied by the high surface area necessary for high storage at elevated pressure. However, as discussed above, the resistant to activation nature of the CNL1 carbon means that even under harsh activation conditions (i.e., KOH/carbon ratio of 4 and 700 – 800 $^oC$) the resulting carbons still retain small micropores to a much greater extent compared to activated carbons derived from other sources (Figure S10), and therefore still have excellent $CO_2$ uptake at low (< 1 bar) pressure.

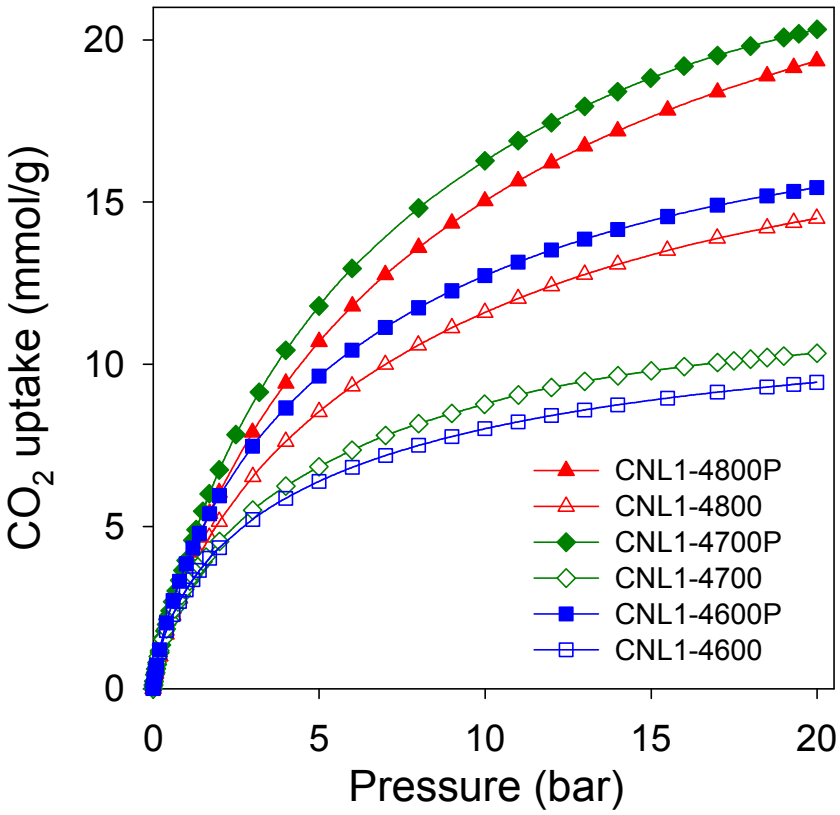


**Figure 6**. $CO_2$ uptake isotherms at 25 ºC and 0 - 20 bar for activated CNL1-4T carbons.

As mentioned above, for comparison purposes and to highlight the advantages of activated carbons from air carbonized biomass, we pyrolysed wood chippings under nitrogen and then activated the resulting carbon to yield CNLW-xT activated carbons. We compared the gravimetric $CO_2$ uptake of the samples derived from 'nitrogen carbonized' wood to similarly activated samples derived from 'air-carbonized' wood, i.e., the CNL1 carbon (Table S5). The comparison showed that activated carbons derived from nitrogen carbonized wood have in all cases lower $CO_2$ uptake at low pressure ($\leq$ 1 bar) due to their less developed microporosity. However, at 20 bar, the $CO_2$ uptake simply depends on the total surface area, and is therefore generally higher for the nitrogen carbonized samples (Table S1). The comparison illustrates the manner in which the concept of air carbonized carbon goes beyond the properties of the activated carbons in directly affecting gas uptake capability.

### 3.4 Packing density of activated CNL1 carbons and volumetric $CO_2$ uptake

The activated CNL1 carbons have attractive gravimetric $CO_2$ uptake as discussed above. On the other hand, due to the hardy nature of the air carbonized CNL1 precursor, the high yielding activated carbons also have unusually high packing density (Table 2) occasioned by apparently low levels of activation and carbon etching. Therefore they exhibit an attractive blend of high gravimetric uptake and high packing density, which are essential for achieving high volumetric $CO_2$ storage. High volumetric $CO_2$ uptake is important for post-combustion capture from flue gas streams because the solid adsorbent material is packed into a column with limited space. Thus, the amount of $CO_2$ stored by the adsorbent per given space (i.e., volume) in the column is an important consideration and can be maximised for storage materials with high packing density. The packing density of the activated CNL1 carbons given in Table 2 was determined by compacting ca. 50 mg of carbon for 10 min at 370 MPa (3700 bar). The compaction did not alter the textural properties or gravimetric $CO_2$ uptake. The packing density is in the range 0.69 – 1.14 g $cm^{-3}$ (Table 2), and generally decreases at higher levels of activation. The packing density of the activated CNL1 carbons is comparable to that of lowly activated carbon monoliths or activated carbons.[73,91] The volumetric uptake of the activated CNL1 carbons is given in Table 2. At low pressure of 0.15 bar, which mimics the conditions for post combustion $CO_2$ capture from flue gas streams, the CNL1-2T carbons have volumetric $CO_2$ uptake of between 44 and 63 g $l^{-1}$ (i.e., 1 – 1.43 mmol $cm^{-3}$), while for CNL1-4T carbons it varies from 24 to 40 g $l^{-1}$ (0.55 to 0.9 mmol $cm^{-3}$). Thus the uptake of CNL1-2T carbons is superior to 40 g $l^{-1}$ (0.9 mmol $cm^{-3}$) for carbon monoliths (sample A1) and 27 g $l^{-1}$ (0.6 mmol $cm^{-3}$) for activated carbon monoliths (sample A3-36), which were recently presented as superior benchmark materials.[91] As shown in Table 2, the activated CNL1 carbons are also vastly superior to an ultra-porous metal organic framework (MOF210)[92] but lower than for a MOF with bare metal sites.[93,94] At 1 bar (Supporting Figure

S19), CNL1-2T carbons achieve uptake of 176 – 207 g $l^{-1}$ (4 – 4.7 mmol $cm^{-3}$), while for CNL1-4T samples (Supporting Figure S20) it is between 102 and 149 g $l^{-1}$ (2.3 and 3.4 mmol $cm^{-3}$). The uptake of CNL2-2T samples is higher than for carbon monoliths A1 (128 g $l^{-1}$ or 2.9 mmol $cm^{-3}$) and A3-36 (157 g $l^{-1}$ or 3.6 mmol $cm^{-3}$),[91] Mg-MOF-74 (144 g $l^{-1}$ or 3.3 mmol $cm^{-3}$)[93,94] and nearly 20 times as much as for MOF210 (10 g $l^{-1}$ or 0.23 mmol $cm^{-3}$).[92] At pressure of 1 bar and above, compactivated carbons outperform their conventionally activated analogues. The superior volumetric $CO_2$ uptake of the best CNL1 carbons is greater than for benchmark materials at pressures above 1 bar as shown in Table 2 and Figure 7.

**Table 2**. Packing density and volumetric $CO_2$ uptake of activated CNL1 carbons. Data for benchmark carbon and metal organic framework (MOF) materials is shown for comparison.

| Sample | Packing density | Volumetric $CO_2$ uptake (g $l^{-1}$) | | | |
|---|---|---|---|---|---|
| | (g $cm^{-3}$) | 0.15 bar | 1 bar | 5 bar | 9 bar |
| CNL1-2600 | 1.14 | 60 | 176 | 320 | 368 |
| CNL1-2600P | 1.11 | 63 | 186 | 337 | 390 |
| CNL1-2700 | 0.98 | 56 | 207 | 429 | 503 |
| CNL1-2700P | 0.90 | 55 | 198 | 428 | 507 |
| CNL1-2800 | 1.01 | 44 | 190 | 444 | 533 |
| CNL1-2800P | 0.95 | 46 | 188 | 451 | 560 |
| CNL1-4600 | 0.92 | 40 | 121 | 259 | 314 |
| CNL1-4600P | 0.87 | 38 | 149 | 369 | 471 |
| CNL1-4700 | 0.89 | 39 | 129 | 268 | 333 |
| CNL1-4700P | 0.78 | 31 | 137 | 407 | 536 |
| CNL1-4800 | 0.70 | 25 | 102 | 263 | 342 |
| CNL1-4800P | 0.69 | 24 | 112 | 326 | 438 |
| Carbon A1[a] | 1.00[a] | 38 | 157 | 278 | 316 |
| Carbon A3-36[a] | 0.87[a] | 27 | 128 | 302 | 378 |
| MOF210[b] | 0.25[c] | 4 | 10 | 38 | 65 |
| Mg-MOF-74[d] | 0.41[e] | 103 | 144 | | |

[a]Data from reference 91. [b]Data from reference 92. [c]Crystal density of MOF210. [d]Data from reference 93. [e]'tapping density' of Mg-MOF-74 from reference 94.

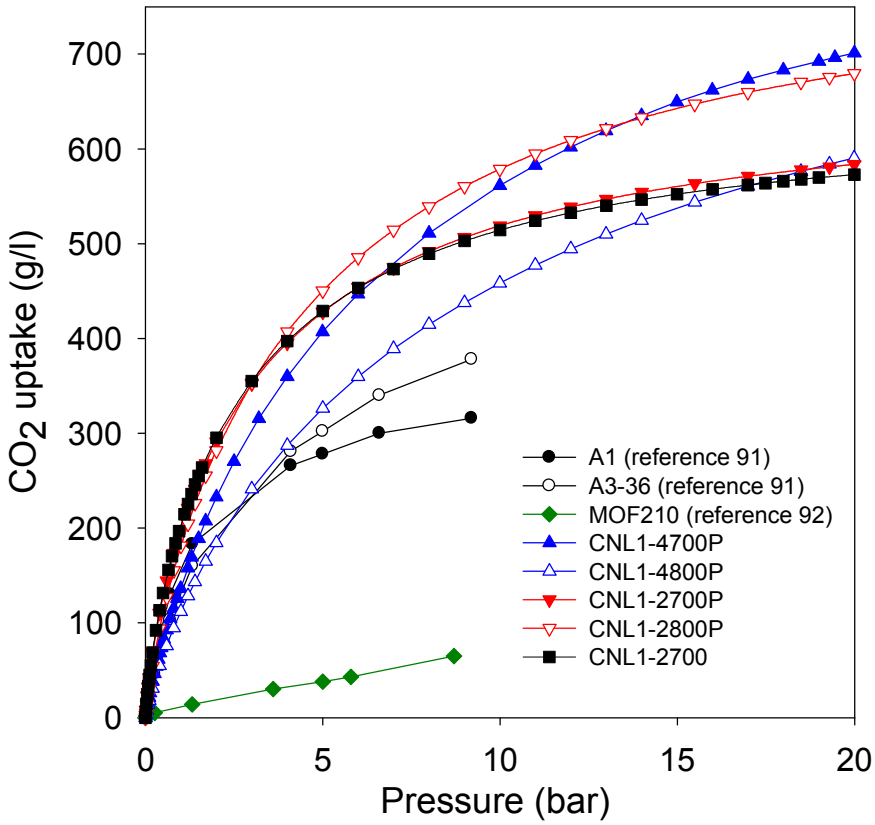


**Figure 7**. Volumetric $CO_2$ uptake for activated or compactivated CNL1 carbons compared with benchmark carbon and MOF materials.

***Working capacity for pressure-swing adsorption (PSA) and vacuum-swing adsorption (VSA)***

At the present time large-scale post-combustion capture and storage of $CO_2$ from flue gas streams is accomplished via the use of liquid amines that chemically bind the $CO_2$. The strong binding between the $CO_2$ and the amines requires thermal treatment to regenerate the later in so-called temperature swing adsorption processes that require large amounts of energy input that render them thermally inefficient.[95,96] The removal of $CO_2$ from flue gas streams may more efficiently be accomplished with solid state adsorbents such as activated carbons via either pressure swing adsorption (PSA) or vacuum swing adsorption (VSA) processes.[97,98] A typical PSA system may adsorb at a pressure of 6 bar and be recycled (i.e., desorb) at 1 bar,

while for VSA systems, adsorption may occur at 1.5 bar and evacuation at ca. 0.05 bar.[99] We therefore explored the performance of the activated CNL1 carbons under conditions that mimic pressure or vacuum swing adsorption processes by estimating their $CO_2$ uptake (as working capacity) with respect to two PSA and VSA scenarios; (i) a pure $CO_2$ stream or (ii) a 20% $CO_2$ stream that more closely mimics flue gas streams that contain ca. 20% $CO_2$. The estimated gravimetric working capacity for the PSA and VSA processes is presented in Table 3. For a pure $CO_2$ stream, the PSA uptake ranges from 3.2 mmol $g^{-1}$ to extremely high values of between 6.5 and up to an exceptional 9.0 mmol $g^{-1}$ for compactivated carbons. As shown in Table 3, such PSA working capacity values of between 6.5 and 9.0 mmol $g^{-1}$ are way above what has previously been reported for the best carbon materials including those derived from organic metal salts (4.3 mmol $g^{-1}$ for CKHP800-1-C5)[63] or from saw dust biochar (3.4 mmol $g^{-1}$ for SD2600P).[73] Indeed, the working capacity of some of the compactivated carbons matches or significantly surpasses that of the best performing materials to date, namely open-metal site containing MOFs (3.5 mmol $g^{-1}$ for Mg-MOF-74 and 7.8 mmol $g^{-1}$ for HKUST-1),[100] and exceeds that of zeolite NaX[101] (Table 3). Under simulated flue gas conditions, the PSA uptake of the activated CNL1 carbons varies between 2.3 and 3.9 mmol $g^{-1}$, which, is amongst the highest so far reported for carbons and, at the higher end, exceeds or matches that of saw dust derived compactivated carbon (4.1 mmol $g^{-1}$ for SD2600P)[73], Mg-MOF-74 (2.1 mmol $g^{-1}$) and HKUST$^{-1}$ (4.5 mmol $g^{-1}$).[100] The estimated VSA uptake is also attractive, reaching 5.3 mmol $g^{-1}$ and 2.2 mmol $g^{-1}$ under pure $CO_2$ and flue gas conditions, respectively. At the high end, the pure $CO_2$ VSA uptake matches that of saw dust derived compactivated carbon (6.0 mmol $g^{-1}$ for SD2600P)[73], Mg-MOF-74 (3.9 mmol $g^{-1}$) and HKUST-1 (6.4 mmol $g^{-1}$).[100]

**Table 3**. Gravimetric and volumetric working capacity for pressure swing adsorption (PSA) and vacuum swing adsorption (VSA) of $CO_2$ on activated CNL1 carbons, and benchmark porous materials at 25 $^oC$ for a pure $CO_2$ gas stream and a 20% partial $CO_2$ pressure flue gas. The values in parentheses are volumetric uptake (in g $l^{-1}$).

| Sample | Pure $CO_2$ uptake[a] (mmol $g^{-1}$) | | Flue gas $CO_2$ uptake[b] (mmol $g^{-1}$) | |
|---|---|---|---|---|
| | PSA | VSA | PSA | VSA |
| CNL1-2600 | 3.2 (161) | 3.7 (186) | 2.4 (120) | 1.7 (85) |
| CNL1-2600P | 3.5 (171) | 3.9 (191) | 2.6 (127) | 1.7 (83) |
| CNL1-2700 | 5.7 (246) | 5.4 (233) | 3.7 (160) | 2.0 (86) |
| CNL1-2700P | 6.5 (273) | 5.0 (198) | 3.9 (154) | 2.2 (87) |
| CNL1-2800 | 6.3 (280) | 5.2 (231) | 3.5 (156) | 1.8 (80) |
| CNL1-2800P | 7.3 (305) | 5.3 (222) | 3.6 (150) | 1.7 (71) |
| CNL1-4600 | 3.8 (154) | 3.4 (138) | 2.3 (93) | 1.4 (57) |
| CNL1-4600P | 6.6 (253) | 4.7 (180) | 3.1 (119) | 1.5 (57) |
| CNL1-4700 | 4.1 (161) | 3.5 (137) | 2.4 (94) | 1.4 (55) |
| CNL1-4700P | 9.0 (309) | 5.2 (179) | 3.5 (120) | 1.5 (52) |
| CNL1-4800 | 6.1 (189) | 4.0 (123) | 2.7 (83) | 1.3 (40) |
| CNL1-4800P | 8.1 (246) | 4.6 (140) | 3.2 (97) | 1.3 (40) |
| CKHP800-1-C5 [c] | 4.3 (125) | 4.4 (128) | 3.0 (87) | 2.0 (58) |
| SD2600P[d] | 3.4 (142) | 6.0 (251) | 4.1 (171) | 2.9 (121) |
| HKUST-1[e] | 7.8 (147) | 6.4 (121) | 4.5 (85) | 1.6 (30) |
| Mg-MOF-74[e] | 3.5 (63) | 3.9 (70) | 2.1 (38) | 4.1 (74) |
| NaX[f] | 1.6 (44) | 2.8 (78) | 1.8 (50) | 2.5 (69) |

[a]1 bar to 6 bar for PSA; 0.05 bar to 1.5 bar for VSA. [b]0.2 bar to 1.2 bar for PSA; 0.01 bar to 0.3 bar for VSA. [c]Data from reference 63. [d]Data from reference 73. [e]Data from reference 100. [f]Data from reference 101.

As discussed above, the activated CNL1 carbons have excellent gravimetric $CO_2$ uptake in PSA and VSA adsorption processes. Given the high density of the carbons, we also calculated the volumetric working capacity for PSA and VSA processes as shown in Table 3. In general the volumetric working capacity of the activated CNL1 carbons is significantly higher than that of the best carbons to date,[63,73] and outperforms that of benchmark zeolite

NaX and MOF materials (Table 3). The CNL1 carbons with the best all-round performance are CNL1-2700, CNL1-2700P, CNL1-2800, CNL1-2800P and CNL1-4900P. For a pure $CO_2$ stream these samples have a PSA volumetric working capacity of between 246 and 309 g $l^{-1}$ compared to 147, 63 and 44 g $l^{-1}$ for $HKUST^{-1}$, Mg-MOF-74 and zeolite NaX, respectively, while their VSA volumetric working capacity is in the range of 179 – 233 g $l^{-1}$ compared to 121, 70 and 78 g $l^{-1}$ for HKUST-1, Mg-MOF-74 and zeolite NaX, respectively. For flue gas conditions, their PSA volumetric working capacity ranges from 120 to 160 g $l^{-1}$, which is significantly above that of the zeolite NaX (50 g $l^{-1}$), HKUST-1 (85 g $l^{-1}$) and Mg-MOF-74 (38 g $l^{-1}$). A similar superiority for some of the CNL1 carbons is observed for the VSA volumetric working capacity (52 – 87 g $l^{-1}$) under flue gas conditions compared to 74, 30 and 69 g $l^{-1}$ for Mg-MOF-74, HKUST-1 and zeolite NaX, respectively.

The volumetric working capacity for pressure swing adsorption (PSA) and vacuum swing adsorption (VSA) of $CO_2$ on activated CNL1 carbon (CNL1-xT) from air carbonized wood was found to be higher, in some cases by up to 50%, than that of similarly activated carbon (CNLW-xT) from wood carbonized under nitrogen (Table S7). The comparison further indicates that the higher packing density of activated carbons derived from air carbonized carbon offers many advantages in terms of gas uptake capability.

## 4. Conclusions

Activated and compactivated carbons were successfully produced for the first time from carbon formed by the burning of wood in air, utilizing KOH as activating agent. The air carbonized carbon, dubbed as CNL1 carbon, was produced from wood during the fire that destroyed the University of Nottingham's partially built all-wood Carbon Neutral Laboratory (CNL) but such carbon may also be prepared in the lab. The air-carbonized carbon was found to be resistant to activation and therefore an excellent precursor for the formation of highly

microporous activated carbons. Indeed, the generated activated carbons are unusual in that they retain microporosity (with surface area of 1121 – 2487 $m^2$ $g^{-1}$) even after severe activation or compactivation along with unprecedentedly high yields (32 – 80 wt%) and packing density (0.7 – 1.14 g $cm^{-3}$). In all cases, the surface area and pore volume of compactivated carbons is higher compared to conventionally activated carbons but with no change in pore size. The porosity of the activated and compactivated CNL1 carbons primarily arises from pore channels of size 5 – 7 Å pores, which favour $CO_2$ uptake and thus the carbons capture up to 5.0 mmol $g^{-1}$ or 4.7 mmol $cm^{-3}$ at 1 bar and 25 $^oC$. The high gravimetric $CO_2$ uptake of the activated CNL1 carbons in combination with high packing density results in exceptional volumetric $CO_2$ storage capacity. Moreover, the nature of their $CO_2$ uptake isotherms is such that the carbons show unprecedented $CO_2$ capture for low pressure swing operations with working capacity for pressure swing adsorption (PSA) of 6 – 9 mmol $g^{-1}$ from a pure $CO_2$ stream (6 to 1 bar) and 3 – 4 mmol $g^{-1}$ from flue gas stream (1.2 to 0.2 bar). The working capacity for vacuum swing adsorption (VSA) is also attractive being in the range 5.0 – 5.4 mmol $g^{-1}$ under pure $CO_2$ (1.5 to 0.05 bar), and 1.8 – 2.2 mmol $g^{-1}$) for flue gas (0.3 to 0.01 bar) conditions. For the best examples, the high gravimetric working capacity translates to exceptional PSA volumetric working capacity of between 246 and 309 g $l^{-1}$, while their VSA volumetric working capacity is in the range of 179 - 233 g $l^{-1}$. For flue gas conditions, their PSA volumetric working capacity ranges from 120 to 160 g $l^{-1}$. We have shown that the all-round performance (gravimetric and volumetric $CO_2$ storage capacity) of the activated CNL1 carbons is significantly higher than that of the best carbons to date, and outperforms that of benchmark zeolite NaX and MOF materials. Our findings suggest a possible use, as activated carbon precursor, for high tonnage carbon residues that are generated during thermal treatment of wood under air or reduced air conditions. The generation of such carbon may also be accomplished under lab-based controlled air-carbonisation conditions.

## Supporting Information

Seven tables with comparative data on elemental composition, yield, porosity and $CO_2$ uptake. Twenty additional figures; photographs of CNL1 carbon, lab-based air-carbonized carbon, XRD patterns, SEM images, TGA curves, comparative nitrogen sorption and pore size distribution curves, comparative trends in porosity of CNL1 carbons, and low to high pressure gravimetric or volumetric $CO_2$ uptake isotherms.


## Acknowledgements

We thank Prof. Andrei Khlobystov for assistance with SEM analysis and Mr. Craig Stoppiello with TEM analysis. We are grateful to Prof Peter Licence (Director of the Carbon Neutral Laboratory), the Nottingham Fire and Rescue Service and Mr. Neil Barnes for sampling of the CNL1 carbon. We thank the government of the Kingdom of Saudi Arabia for funding a PhD studentship for Norah Balahmar.


## 5. References


1. http://www.bbc.co.uk/news/uk-england-nottinghamshire-30751431. March 2016.
2. https://www.nottingham.ac.uk/Chemistry/Research/Centre-for-Sustainable-Chemistry.aspx March 2016.
3. A. Wennerberg, T.M. O'Grady, US Patent no 4,082,694 (1978).
4. D. Li, T. Ma, R. Zhang, Y. Tian and Y. Qiao, *Fuel,* 2015, **139**, 68.
5. Y. Guo, S. Yang, K. Yu, J. Zhao, Z. Wang and H. Xu, *Mater. Chem. Phys.*, 2002, **74**, 320.
6. L. Muniandy, F. Adam, A. R. Mohamed and E. Ng, *Micropor. Mesopor. Mater.*, 2014, **197**, 316.
7. Z. Hu and M. P. Srinivasan, *Micropor. Mesopor. Mater.*, 1999, **27**, 11.
8. Y. J. Hwang, S. K. Jeong, J. S. Shin, K. S. Nahm and A. M. Stephan. *J. Alloys Comp.*, 2008, **448**, 141.
9. F. Wu, R. Tseng and R. Juang, *Sep. Purif. Technol.*, 2005, **47**, 10.

10. F. Wu and R. Tseng, *J. Colloid Interface Sci.*, 2006, **294**, 21.
11. S. I. Tsyganova, *Wood Sci. Technol.,* 2013, **1**, 77.
12. M. Molina-Sabio and F. Rodriguez-Reinoso, *Colloids Surf., A,* 2004, **241**, 15.
13. J. Song, W. Shen, J. Wang and W. Fan, *Carbon,* 2014, **69**, 255.
14. M. Sevilla and A. B. Fuertes, *Energy Environ. Sci.,* 2011, **4**, 1765.
15. M. A. Lillo-Rodenas, D. Cazorla-Amoros and A. Linares-Solano, *Carbon,* 2003, **41**, 267.
16. D. Lozano-Castello, J. M. Calo, D. Cazorla-Amoros and A. Linares-Solano, *Carbon*, 2007, **45**, 2529.
17. M. A. Lillo-Rodenas, D. Cazorla-Amoros and A. Linares-Solano, *Carbon,* 2004, **42**, 1371.
18. M. J. Bleda-Martinez, J. A. Macia-Agullo, D. Lozano-Castello, E. Morallon, D. Cazorla-Amoros and A. Linares-Solano, *Carbon, 2005,* **43**, 2677.
19. M. Sevilla, N. Alam and R. Mokaya, *J. Phys. Chem. C,* 2010, **114**, 11314.
20. Y. Gogotsi, C. Portet, S. Osswald, J. M. Simmons, T. Yildirim, G. Laudisio and J. E. Fischer, *Int. J. Hydrogen Energy*, 2009, **34**, 6314.
21. M. Sevilla, R. Foulston and R. Mokaya, *Energy Environ. Sci.,* 2010, **3**, 223.
22. Y. Zhu, S. Murali, M. D. Stoller, K. J. Ganesh, W. Cai, P. J. Ferreira, A. Pirkle, R. M. Wallace, K. A. Cychosz, M. Thommes, D. Su, E. A. Stach and R. S. Ruoff, *Science*, 2011, **332**, 1537.
23. E. Raymundo-Piñero, D. Cazorla-Amorós, A. Linares-Solano, S. Delpeux, E. Frackowiak, K. Szostak and F. Béguin, *Carbon*, 2002, **40**, 1614.
24. M. Sevilla and R. Mokaya, *Energy Environ. Sci.,* 2014, **7**, 1250.
25. M. Sevilla and R. Mokaya, *J. Mater. Chem.* 2013, **21**, 4727.
26. M. C. Baquero, L. Giraldo, J. C. Moreno, F. Suárez-García, A. Martínez-Alonso and J. M. D. Tascón, *J. Anal. Appl. Pyrolysis*, 2003, **70**, 779.
27. M. Jagtoyen and F. Derbyshire, *Carbon*, 1998, **7**, 1085.
28. W. Xing, C. Liu, Z. Zhou, L. Zhang, J. Zhou, S. Zhuo, Z. Yan, H. Gao, G. Wang and S. Z. Qiao, *Energy Environ. Sci.*, 2012, **5**, 7323.
29. B. Adeniran and R. Mokaya, *Chem. Mater.* 2016, **28**, 994.
30. N. P. Wickramaratne and M. Jaroniec, *J. Mater. Chem. A.,* 2013, **1**, 112.
31. K. Yang, J. Peng, C. Srinivasakannan, L. Zhang, H. Xia and X. Duan, *Bioresource Technol.*, 2010, **101**, 6163.
32. F. Caturla, M. Molina-Sabio and F. Rodríguez-Reinoso, *Carbon,* 1991, **29**, 999.

33. Z. Hu, M.P. Srinivasan and Y. Ni, *Carbon,* 2001, **39**, 877.
34. M. M. Titirici, R. J. White, C. Falco and M. Sevilla, *Energy Environ. Sci*. 2012, **5,** 6796.
35. M. Sevilla and A. B. Fuertes, *Carbon*, 2009, **47**, 2281.
36. M. M. Titirici and M. Antonietti, *Chem. Soc. Rev*. 2010, **39**, 103.
37. A. C. Pastor, F. Rodríguez-Reinoso, H. Marsh and M. A. Martínez, *Carbon*, 1999, **37**, 1275.
38. R. F. Schwenker and E. Pacsu, *Ind. Eng. Chem.*, 1958, **50**, 91.
39. J. Chmiola, G. Yushin, Y. Gogotsi, C. Portet, P. Simon and P. L. Taberna, *Science*, 2006, **313**, 1760.
40. J. Huang, B. G. Sumpter and V. Meunier, *Chem. Eur. J.,* 2008, **14**, 6614.
41. M. A. de la Casa-Lillo, F. Lamari-Darkrim, D. Cazorla-Amorós and A. Linares-Solano, *J. Phys. Chem. B.,* 2002, **106**, 10930.
42. J. S. Im, S. J. Park, T. J. Kim, Y. H. Kim and Y-S. Lee, *J. Colloid Interface Sci.,* 2008, **318**, 42.
43. E. Masika and R. Mokaya, *Energy Environ. Sci*., 2014, **7**, 427.
44. E. Masika and R. Mokaya, *J. Phys. Chem. C*, 2012, **116***,* 25734.
45. N. Alam and R. Mokaya, *Energy Environ. Sci*., 2010, **3**, 1773.
46. A. Yamasaki, *J. Chem. Eng. Jpn.*, 2003, **36**, 361.
47. S. Choi, J. H. Drese and C. W. Jones, *ChemSusChem*, 2009, **2**, 796.
48. H. Yang, Z. Xu, M. Fan, R. Gupta, R. B. Slimane, A. E. Bland, I. Wright, *J. Environ. Sci.,* 2008, **20**, 14.
49. R. E. Morris, P. S. Wheatley, *Angew. Chem. Int. Ed.*, 2008, **47** 4966.
50. Y. Liu, J. Wilcox, *Environ. Sci. Technol.*, 2012, **46**, 1940.
51. M. Sevilla, P. Valle-Vigón, A. B. Fuertes, *Adv. Funct. Mater.*, 2011, **21**, 2781.
52. M. Sevilla, R. Mokaya, A. B. Fuertes, *Energy Environ. Sci.*, 2011, **4** 1400.
53. H. S. Teng, L. Y. Hsu, *Ind. Eng. Chem. Res*, 1999, **38**, 2947.
54. M. X. Fang, D. K. Shen, Y. X. Li, C. J. Yu, Z. Y. Luo, K. F. Cen, *J. Anal. Appl. Pyrolysis*, 2006, **77**, 22.
55. M. Sevilla, R. Mokaya and A. B. Fuertes, *Energy Environ. Sci.*, 2011, **4**, 2930.
56. B. Adeniran and R. Mokaya, *Nano Energy*, 2015, **16***,* 173.
57. W. Sangchoom and R. Mokaya, *ACS Sust. Chem. Eng*., 2015, **3**, 1658.
58. C. L. Magnun, K. R. Benak, J. Economy, K. L. Foster, *Carbon*, 2001, **39**, 1809.
59. G. T. K. Fey, C. L. Chen, *J. Power Sources*, 1998, **76**, 156.
60. K. S. W. Sing, D. H. Everett, R. A. W. Haul, L. Moscou, R. A. Pierotti, J. Rouquerol and

T. Siemieniewska, *Pure Appl. Chem.,* 1985, **57**, 603.
61. B. Adeniran and R. Mokaya, *J. Mater. Chem. A*, 2015, **3**, 5148.
62. N. P. Wickramaratne and M. Jaroniec, *ACS Appl. Mater. Interfaces*, 2013, **5**, 1849.
63. B. Adeniran, E. Masika and R. Mokaya, *J. Mater. Chem. A*, 2014, **2**, 14696.
64. X. Fan, L. Zhang, G. Zhang, Z. Shu and J. Shi, *Carbon*, 2013, **61**, 423.
65. Z. Zhang, J. Zhou, W. Xing, Q. Xue, Z. Yan, S. Zhuo and S. Z. Qiao, *Phys. Chem. Chem. Phys.,* 2013, **15**, 2523.
66. H. Wei, S. Deng, B. Hu, Z. Chen, B. Wang, J. Huang and G. Yu, *ChemSusChem*, 2012, **5**, 2354.
67. J. A. Maciá-Agulló, B. C. Moore, D. Cazorla-Amorós and A. Linares-Solano, *Carbon*, 2004, **42**, 1367.
68. A. Almasoudi and R. Mokaya, *J. Mater. Chem. A*, 2014, **2**, 10960.
69. A. Almasoudi and R. Mokaya, *Micropor. Mesopor. Mater.*, 2014, **195**, 258.
70. C. Robertson and R. Mokaya, *Micropor. Mesopor. Mater.,* 2013, **179**, 151.
71. M. Sevilla, A. B. Fuertes and R. Mokaya, *Int. J. Hydrogen Energy*, 2011, **36**, 15658.
72. A. Almasoudi and R. Mokaya. *J. Mater. Chem.*, 2012, **22**, 146.
73. N. Balahmar, A. C. Mitchell, and R. Mokaya, *Adv. Energy Mater.*, **2015**, *5*, 1500867.
74. H. M. Coromina, D. A. Walsh and R. Mokaya, *J. Mater. Chem. A*, 2016, **4**, 280.
75. W. M. A. W. Daud and W. S. W. Ali, *Bioresour. Technol*. 2004, **93**, 63.
76. R. K. Sharma, J. B. Wooten, V. L Baliga, X. Lin, W. G. Chan and M. R. Hajaligol, *Fuel* 2004, **83**, 1469.
77. Z. Fang, T. Sato, R. L. Smith Jr, H. Inomata, K. Arai and J. A. Kozinski, *Biores. Technol.*, 2008, **99**, 3424.
78. M. Bbebu and C. Vasile, *Cellulose Chem. Technol*., 2010, **44**, 353.
79. H. Yang, R. Yan, H. Chen, C. Zheng, D. H. Lee and D. T. Liang, *Energy Fuels*, 2006**, 20***,* 388.
80. M. J. Antal, S. G. Allen, X. Dai, B. Shimizu, M. S. Tam and M. Gronli, *Ind. Eng. Chem. Res.*, 2000, **39**, 4024.
81. M. J. Antal, E. Croiset, X. Dai, C. DeAlmeida, W. S-L. Mok, N. Norberg, J-R. Richard and M. Al Majthoub, *Energy Fuels*, 1996, **10**, 652.
82. M. J. Antal, *Patent no. US 6,790,317 B2*, 2004. http://www.google.co.uk/patents/US6790317
83. Y. D. Xia, R. Mokaya, G. S. Walker and Y. Q. Zhu, *Adv. Energy Mater.*, 2011, **1**, 678.
84. M. Nandi, K. Okada, A. Dutta, A. Bhaumik, J. Maruyama, D. Derksa and H. Uyama, *Chem. Commun*., 2012, **48**, 10283.

85. J. Silvestre-Albero, A. Wahby, A. Sepulveda-Escribano, M. Martinez-Escandell, K. Kaneko and F. Rodriguez-Reinoso, *Chem. Commun*., 2011, **47**, 6840.
86. G. Srinivas, J. Burress and T. Yildirim, *Energy Environ. Sci*., 2012, **5**, 6453.
87. A. Wahby, J. M. Ramos-Fernandez, M. Martnez-Escandell, A. Sepulveda-Escribano, J. Silvestre-Albero and F. Rodriguez-Reinoso, *ChemSusChem*, 2010, **3**, 974.
88. D. Lee, C. Zhang, C. Wei, B. L. Ashfeld and H. Gao, *J. Mater. Chem. A*, 2013, 1, 14862.
89. J. D. Figueroa, T. Fout, S. Plasynski, H. McIlvried and R. D. Srivastava, *Int. J. Greenhouse Gas Control*, 2008, **2**, 9.
90. Z. Zhang, K. Wang, J. D. Atkinson, X. Yan, X. Li, M. J. Rood and Z. Yan, *J. Hazard. Mater*., 2012, **229–230**, 183.
91. J. P. Marco-Lozar, M. Kunowsky, F. Suarez-Garcia, J. D. Carruthers and A. Linares-Solano, *Energy Environ. Sci*., 2012, **5**, 9833.
92. H. Furukawa, N. Ko, Y. B. Go, N. Aratani, S. B. Choi, E. Choi, A. O. Yazaydin, R. Q. Snurr, M. O'Keeffe, J. Kim and O. M. Yaghi, *Science*, 2010, **329**, 424.
93. S. R. Caskey, A. G. Wong-Foy and A. J. Matzger, *J. Am. Chem. Soc*., 2008, **130**, 10870.
94. Y. Peng, V. Krungleviciute, I. Eryazici, J. T. Hupp, O. K. Farha and T. Yildirim, *J. Am. Chem. Soc*. 2013, **135**, 11887.
95. G. T. Rochelle, *Science*, 2009, **325**, 1652.
96. B. Smit, J. R. Reimer, C. M. Oldenburg and I. C. I. C. Bourg, *Introduction to Carbon Capture and Sequestration*, Imperial College Press, London, 1st edn, 2014.
97. E. S. Kikkinides, S. H. Cho and R. T. Yang, *Ind. Eng. Chem. Res.,* 1993, **32**, 2714.
98. D. Ko, R. Siriwardane and L. Biegler, *Ind. Eng. Chem. Res.* 2005, **44**, 8084.
99. L. Wang, Y. Yang, W. Shen, X. Kong, P. Li, J. Yu and A. E. Rodrigues, *Ind. Eng. Chem. Res.,* 2013, **52**, 7947.
100. J. M. Simmons, H. Wu, W. Zhou and T. Yildirim, *Energy Environ. Sci*., 2011, **4**, 2177.
101. Y. Belmabkhout, G. Pirngruber, E. Jolimaitre and A. Methivier, *Adsorption*, 2007, **13**, 341.

## Graphical Abstract

Air carbonized carbon from biomass is resistant to activation and generates high yields (up to 80 wt%) of high packing density (0.7 – 1.14 g $cm^{-3}$) activated carbons that exhibit enhanced gravimetric $CO_2$ uptake of up to 5.0 mmol $g^{-1}$ at 25 °C and 1 bar. High gravimetric uptake in combination with high packing density results in exceptional volumetric $CO_2$ storage capacity especially for pressure or vacuum swing adsorption.

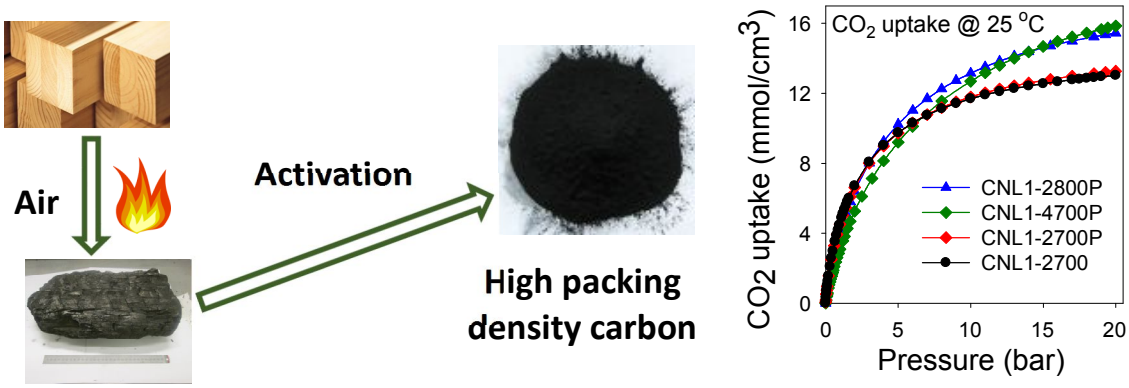

*Supporting Information*

# High yield and high packing density porous carbons for unprecedented $CO_2$ capture from the first attempt at activation of *air-carbonized* biomass

Ephraim Haffner-Staton, Norah Balahmar, Robert Mokaya*

School of Chemistry, University of Nottingham, University Park, Nottingham NG7 2RD, U. K.

*E-mail: r.mokaya@nottingham.ac.uk (R. Mokaya)*

## Laboratory preparation of biomass-derived air-carbonised carbons

Motivated by the attractive properties of the 'air carbonised' CNL carbon, we explored the possibility of deliberately generating such carbon under controlled lab conditions. The following procedures have proved successful in carbonizing biomass in the presence of air;

**Method 1:** Between 2 and 10 g of biomass (wood chippings) was dried in a furnace and heated (at a ramp rate of 10 $^{o}$C min$^{-1}$) to ca. 400 $^{o}$C under a flow 10% air in nitrogen. The temperature was held at the final temperature for 1 h (under a flow 10% air in nitrogen) and then cooled (under a flow of nitrogen only) to room temperature.

**Method 2:** Between 2 and 10 g of biomass (wood chippings) was dried in a furnace and heated (at a ramp rate of 10 $^{o}$C min$^{-1}$) to the target temperature (between 350 and 450 $^{o}$C). At the target temperature, the gas flow was switched to air only for 10 minutes and then the sample cooled down to room temperature under nitrogen flow.

**Table S1**. Elemental composition of CNL1 carbon compared to biochar and hydrochar from other biomass precursors.

| Sample | Carbonisation conditions | Carbonisation temperature (°C) | C (wt%) | H (wt%) | N (wt%) | O (wt% | Reference |
|---|---|---|---|---|---|---|---|
| CNL1 carbon | Air | | 77.7 | 3.1 | 0 | 19.2 | This work |
| Rice husk char | $N_2$ | 400 | 71.5 | / | / | 25.5 | 1 |
| Cherry stone char | Ar | 400 | 77.6 | 4.6 | 0.8 | 16.9 | 2 |
| Beech pellet char | Ar | 800 | 82.7 | 2.0 | 0.4 | 14.9 | 3 |
| Tire char | $O_2$ free | 450 | 72.5 | 4.7 | 4.8 | 15.3 | 4 |
| Lignite char | $N_2$ | 475 | 65.0 | 2.4 | 0.9 | 18.2 | 5 |
| Lignin hydrochar | Water | 390 | 66.6 | 5.1 | 0 | 28.3 | 6 |
| Saw-dust hydrochar | Water | 250 | 69.3 | 6.8 | 0 | 23.9 | 7 |


1. L. Muniandy, F. Adam, A. R. Mohamed and E. Ng, *Micropor. Mesopor. Mater.*, 2014, **197**, 316.
2. R. Pietrzak, P. Nowicki, J. Kaźmierczak, I. Kuszyńska, J. Goscianska and J. Przepiórski, *Chem. Eng. Res. Des.,* 2014, **92**, 1187.
3. K. Zeng, D. P. Minh, D. Gauthier, E. Weiss-Hortala, A. Nzihou and G. Flamant, *Bioresource Technol.*, 2015, **182**, 114.
4. V. Makrigianni, A. Giannakas, C. Daikopoulos, Y. Deligiannakis and I. Konstantinou, *Appl. Catal., B,* 2015, **174**, 244.
5. G. Chattopadhyaya, D. G. Macdonald, N. N. Bakshi, J. S. S. Mohammadzadeh and A. K. Dalai, *Fuel Proces. Technol.*, 2006, **87**, 997.
6. W. Sangchoom and R. Mokaya, *ACS Sust. Chem. Eng*., 2015, **3**, 1658.
7. B. Adeniran and R. Mokaya, *Nano Energy*, 2015, **16***,* 173.

**Table S2**. Carbon yield of activated carbons derived from various precursors.

| Activation conditions | | Yield[a] from various precursors | | |
|---|---|---|---|---|
| KOH/carbon ratio | Temperature (°C) | CNL1 carbon | Lignin hydrochar[b] | Polypyrrole[c,d] |
| 2 | 600 | 80 | 36 | 45 |
| 2 | 700 | 65 | 27 | 34 |
| 2 | 800 | 52 | 21 | 22 |
| 4 | 600 | 68 | 20 | 18 |
| 4 | 700 | 53 | 19 | 20 |
| 4 | 800 | 32 | 15 | 15 |

[a] g of activated carbon/100 g hydrochar.
[b] Data from ref. 57; W. Sangchoom and R. Mokaya, *ACS Sust. Chem. Eng*., 2015, **3**, 1658.
[c] Data from ref 55; M. Sevilla, R. Mokaya and A. B. Fuertes, *Energy Environ. Sci.*, 2011, **4**, 2930.
[d] Data from ref. 56; B. Adeniran and R. Mokaya, *Nano Energy*, 2015, **16**, 173.

**Table S3**. Textural properties of activated carbons derived from CNL1 carbon at activation temperature of 800 ºC and KOH/carbon ratio of 2 or 4 compared to activated carbons from lignin hydrochar (LAC), grass hydrochar (ACGR), carbon nanotube composites (CN) and polypyrrole (Py).

| Sample | Surface area[a] ($m^2$ $g^{-1}$) | Pore volume[b] ($cm^3$ $g^{-1}$) | Pore size[c] (Å) |
|---|---|---|---|
| CNL1-2800 | 1326 (1263) | 0.60 (0.55) | 6/8.5/13 |
| LAC2800 | 1924 (1839) | 0.95 (0.87) | 7/9/13 |
| ACGR2800 | 2735 (2083) | 1.47 (0.94) | 6.5/9/12 |
| CN2800 | 2925 (2538) | 1.56 (1.18) | 6/8/11/21 |
| Py2800 | 3410 (2530) | 1.94 (1.21) | 12/25 |
| CNL1-4800 | 2183 (1886) | 1.05 (0.84) | 6.5/8.5/16 |
| LAC4800 | 3235 (1978) | 1.77 (0.93) | 8/11/27 |
| ACGR4800 | 2957 (1578) | 1.72 (0.75) | 8/12/27 |
| CN4800 | 3802 (33) | 2.98 (0.22) | 8/12/34 |
| Py4800 | 3450 (1910) | 2.57 (1.22) | 13/34 |

The values in the parenthesis refer to: [a]micropore surface area and [b]micropore volume. [c]pore size distribution maxima obtained from NLDFT analysis.

LAC data from ref. 57; W. Sangchoom and R. Mokaya, *ACS Sust. Chem. Eng*., 2015, **3**, 1658.
ACGR data from ref. 74; H. M. Coromina, D. A. Walsh and R. Mokaya, *J. Mater. Chem. A*, 2016, **4**, 280.
CN data from ref. 61; B. Adeniran and R. Mokaya, *J. Mater. Chem. A*, 2015, **3**, 5148.
Py data from ref. 55; M. Sevilla, R. Mokaya and A. B. Fuertes, *Energy Environ. Sci.*, 2011, **4**, 2930.

**Table S4**. Textural properties of activated carbons from various precursors.

| Activation conditions[a] | Precursor | | | | | | | | | |
|---|---|---|---|---|---|---|---|---|---|---|
| | CNL1 carbon | | Lignin hydrochar[g] | | Grass Hydrochar[h] | | CNT composites[i] | | Polypyrrole[j] | |
| | SA[b] | PV[c] | SA | PV | SA | PV | SA | PV | SA | PV |
| | *μSA*[d] | *μPV*[e] | *μSA* | *μPV* | *μSA* | *μPV* | *μSA* | *μPV* | *μSA* | *PV* |
| | **(%μ)**[f] | **(%μ)** | **(%μ)** | **(%μ)** | **(%μ)** | **(%μ)** | **(%μ)** | **(%μ)** | **(%μ)** | **(%μ)** |
| 2/600 | 1190 | 0.55 | 1157 | 0.59 | 1048 | 0.51 | 1479 | 0.83 | 1700 | 0.88 |
| | *1107* | *0.49* | *1123* | *0.54* | *975* | *0.43* | *1400* | *0.67* | | *0.74* |
| | **(93)** | **(89)** | **(97)** | **(92)** | **(93)** | **(84)** | **(95)** | **(81)** | | **(84)** |
| 2/700 | 1399 | 0.63 | 1551 | 0.77 | 1512 | 0.74 | 2102 | 1.18 | 2940 | 1.37 |
| | *1343* | *0.59* | *1502* | *0.72* | *1426* | *0.62* | *1987* | *0.95* | *2660* | *1.14* |
| | **(96)** | **(93)** | **(97)** | **(94)** | **(94)** | **(84)** | **(95)** | **(81)** | **(90)** | **(83)** |
| 2/800 | 1326 | 0.60 | 1924 | 0.95 | 2735 | 1.47 | 2925 | 1.56 | 3410 | 1.94 |
| | *1263* | *0.55* | *1839* | *0.87* | *2083* | *0.94* | *2538* | *1.18* | *2530* | *1.21* |
| | **(95)** | **(92)** | **(96)** | **(92)** | **(76)** | **(64)** | **(87)** | **(76)** | **(74)** | **(62)** |
| 4/600 | 1121 | 0.53 | 1820 | 0.97 | 2396 | 1.15 | 2051 | 1.09 | 2050 | 1.03 |
| | *1021* | *0.45* | *1627* | *0.75* | *2182* | *0.96* | *1752* | *0.82* | *1670* | *0.74* |
| | **(91)** | **(85)** | **(89)** | **(82)** | **(91)** | **(83)** | **(85)** | **(75)** | **(81)** | **(72)** |
| 4/700 | 1280 | 0.65 | 2038 | 1.00 | 3144 | 1.56 | 3202 | 2.14 | 3480 | 2.39 |
| | *1191* | *0.56* | *1832* | *0.84* | *2753* | *1.23* | *1106* | *0.50* | *2190* | *1.18* |
| | **(93)** | **(86)** | **(90)** | **(84)** | **(88)** | **(79)** | **(35)** | **(23)** | **(63)** | **(49)** |
| 4/800 | 2183 | 1.05 | 3235 | 1.77 | 2957 | 1.72 | 3802 | 2.98 | 3450 | 2.57 |
| | *1886* | *0.84* | *1978* | *0.93* | *1578* | *0.75* | *33* | *0.22* | *1910* | *1.22* |
| | **(86)** | **(80)** | **(61)** | **(53)** | **(53)** | **(44)** | **(1)** | **(7)** | **(55)** | **(47)** |

[a] Activation conditions given as x/T, where x is KOH/carbon ratio and T is temperature (°C).
[b] SA is total surface area.
[c] PV is total pore volume.
[d] μSA is micropore surface area.
[e] μPV is micropore volume.
[f] (μ%) is micropore surface area or pore volume as a percentage of total surface or pore volume, respectively.
[g] Data from ref. 57; W. Sangchoom and R. Mokaya, *ACS Sust. Chem. Eng*., 2015, **3**, 1658.
[h] Data from ref. 74; H. M. Coromina, D. A. Walsh and R. Mokaya, *J. Mater. Chem. A*, 2016, **4**, 280.
[i] Data from ref. 61; B. Adeniran and R. Mokaya, *J. Mater. Chem. A*, 2015, **3**, 5148.
[j] Data from ref. 55; M. Sevilla, R. Mokaya and A. B. Fuertes, *Energy Environ. Sci.*, 2011, **4**, 2930.

**Table S5**. Yield, textural properties and $CO_2$ uptake of activated CNL1 carbon (CNL1-xT) from air carbonized wood compared to a similarly activated carbon (CNLW-xT) from wood carbonized under nitrogen. (x is KOH/carbon ratio, and T is activation temperature).

| Sample | Yield[a] (wt%) | Surface area[b] ($m^2$ $g^{-1}$) | Pore volume[c] ($cm^3$ $g^{-1}$) | Pore size[d] (Å) | $CO_2$ uptake[e] (mmol $g^{-1}$) | | |
|---|---|---|---|---|---|---|---|
| | | | | | 0.15 bar | 1 bar | 20 bar |
| **CNL1-2700** | **65** | **1399 (1343)** | **0.63 (0.59)** | **6/8.5/12** | **1.3** | **4.8** | **13.4** |
| CNLW-2700 | 44 | 1592 (1289) | 0.75 (0.51) | 7/9/14 | 1.2 | 4.3 | 12.5 |
| **CNL1-2800** | **52** | **1326 (1263)** | **0.60 (0.55)** | **6/8.5/13** | **1.0** | **4.3** | **14.1** |
| CNLW-2800 | 33 | 2144 (1361) | 1.27 (0.64) | 7/12/25 | 0.8 | 3.5 | 20.1 |
| **CNL1-4700** | **53** | **1280 (1191)** | **0.65 (0.56)** | **6.5/8.5/15** | **1.0** | **3.3** | **10.5** |
| CNLW-4700 | 34 | 2250 (2108) | 0.98 (0.89) | 12/15 | 0.9 | 2.6 | 19.5 |
| **CNL1-4800** | **32** | **2183 (1886)** | **1.05 (0.84)** | **6.5/8.5/16** | **0.8** | **3.3** | **14.5** |
| CNLW-4800 | 21 | 2791 (881) | 1.75 (0.50) | 8/12/29 | 0.5 | 2.8 | 21.6 |

[a]The yield is based on starting weight of CNL1 carbon. The values in the parenthesis refer to: [b]micropore surface area and [c]micropore volume. [d]Pore size distribution maxima obtained from NLDFT analysis. [e]$CO_2$ uptake at 25 $^oC$ and various pressures (i.e., 0.15 bar, 1 bar and 20 bar).

**Table S6**. Textural properties of CNL1 carbon compared to biomass (wood chippings) derived lab generated air carbonised carbon.

| Sample | Surface area[a] ($m^2$ $g^{-1}$) | Pore volume[b] ($cm^3$ $g^{-1}$) | Pore size[c] (Å) |
|---|---|---|---|
| CNL1 carbon | 100 (79) | 0.60 (0.035) | 7/12 |
| Lab air carbonised carbon | 122 (85) | 0.07 (0.037) | 7/12 |

The values in the parenthesis refer to: [a]micropore surface area and [b]micropore volume. [c]pore size distribution maxima obtained from NLDFT analysis.

**Table S7**. Gravimetric and volumetric working capacity for pressure swing adsorption (PSA) and vacuum swing adsorption (VSA) of $CO_2$ on activated CNL1 carbon (CNL1-xT) from air carbonized wood compared to similarly activated carbon (CNLW-xT) from wood carbonized under nitrogen. (x is KOH/carbon ratio, and T is activation temperature). The $CO_2$ uptake is at 25 $^oC$ for a pure $CO_2$ gas stream and a 20% partial $CO_2$ pressure flue gas. The values in parentheses are volumetric uptake or working capacity (in g $l^{-1}$).

| Sample | Packing density (g $cm^{-3}$) | Pure $CO_2$ uptake[a] (mmol $g^{-1}$) | | Flue gas $CO_2$ uptake[b] (mmol $g^{-1}$) | |
|---|---|---|---|---|---|
| | | PSA | VSA | PSA | VSA |
| **CNL1-2700** | **0.98** | **5.7 (246)** | **5.4 (233)** | **3.7 (160)** | **2.0 (86)** |
| CNLW-2700 | 0.71 | 5.5 (172) | 5.0 (156) | 3.5 (109) | 2.0 (63) |
| **CNL1-2800** | **1.01** | **6.3 (280)** | **5.2 (231)** | **3.5 (156)** | **1.8 (80)** |
| CNLW-2800 | 0.65 | 6.5 (186) | 4.4 (126) | 3.2 (92) | 1.3 (38) |
| **CNL1-4700** | **0.89** | **4.1 (161)** | **3.5 (137)** | **2.4 (94)** | **1.4 (55)** |
| CNLW-4700 | 0.47 | 5.0 (103) | 3.2 (66) | 2.1 (43) | 1.3 (27) |
| **CNL1-4800** | **0.70** | **6.1 (189)** | **4.0 (123)** | **2.7 (83)** | **1.3 (40)** |
| CNLW-4800 | 0.41 | 7.1 (128) | 3.7 (67) | 2.8 (51) | 1.1 (20) |

[a]1 bar to 6 bar for PSA; 0.05 bar to 1.5 bar for VSA. [b]0.2 bar to 1.2 bar for PSA; 0.01 bar to 0.3 bar for VSA.


**Supporting Figure S1**. Charred wooden beam from Carbon Neutral Laboratory (CNL1).

**Supporting Figure S2**. Cross section of charred wooden beam from Carbon Neutral Laboratory (CNL1).

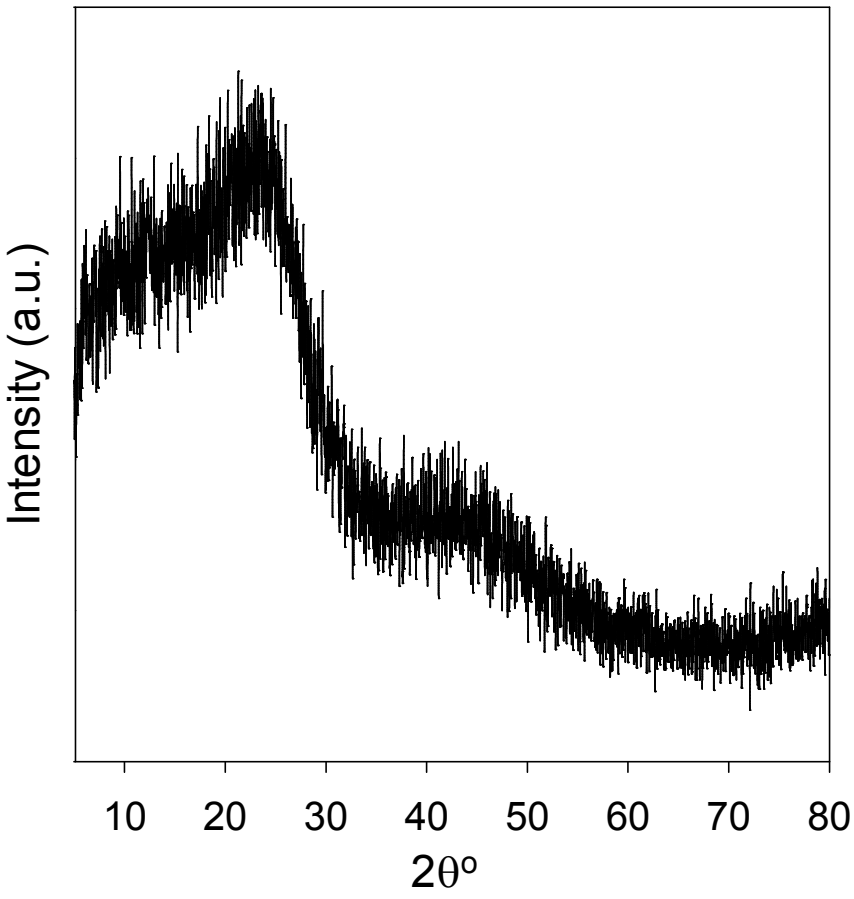


**Supporting Figure S3**. Powder XRD pattern of CNL1 carbon.

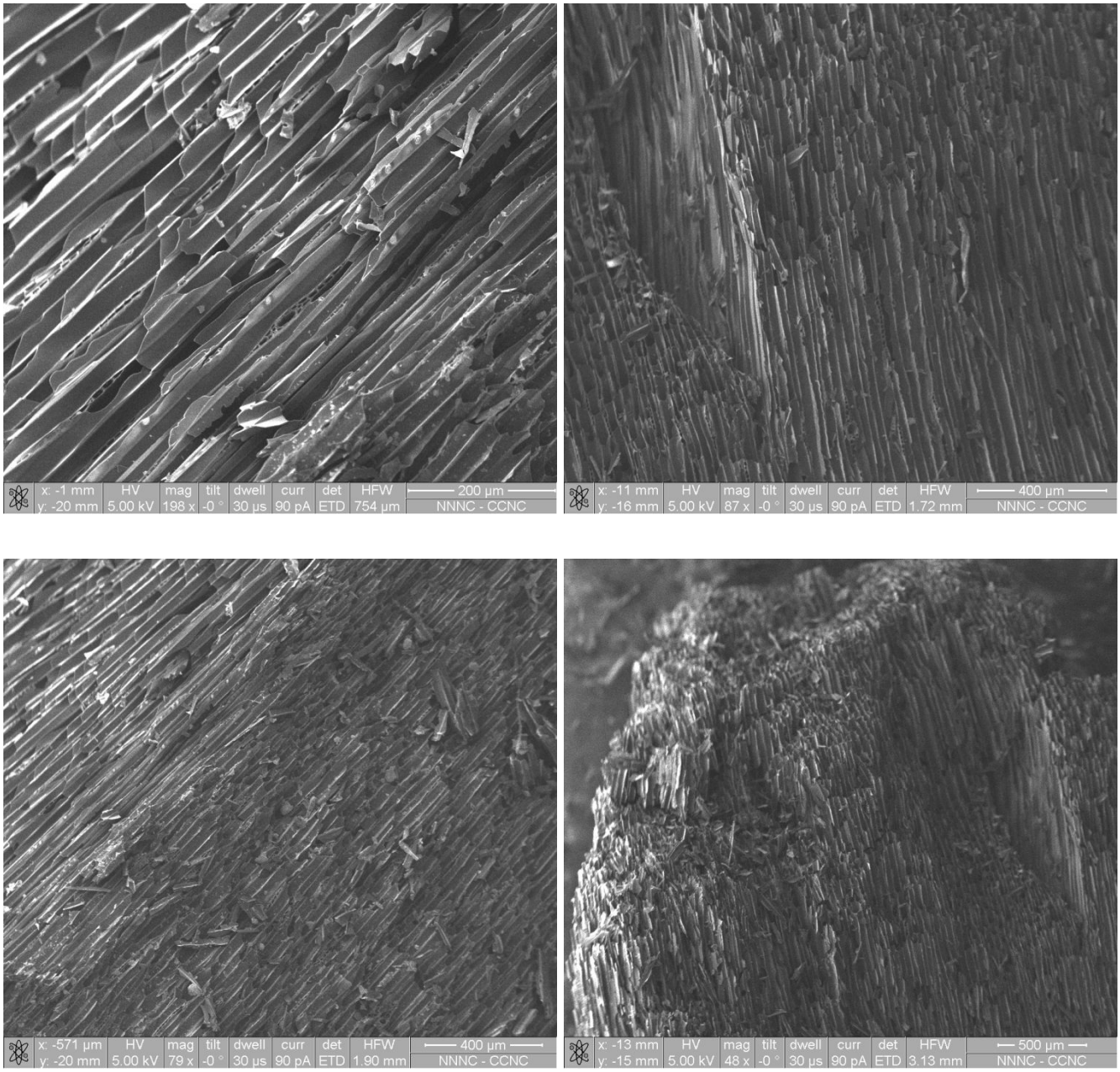


**Supporting Figure S4**. SEM images of CNL1 carbon.

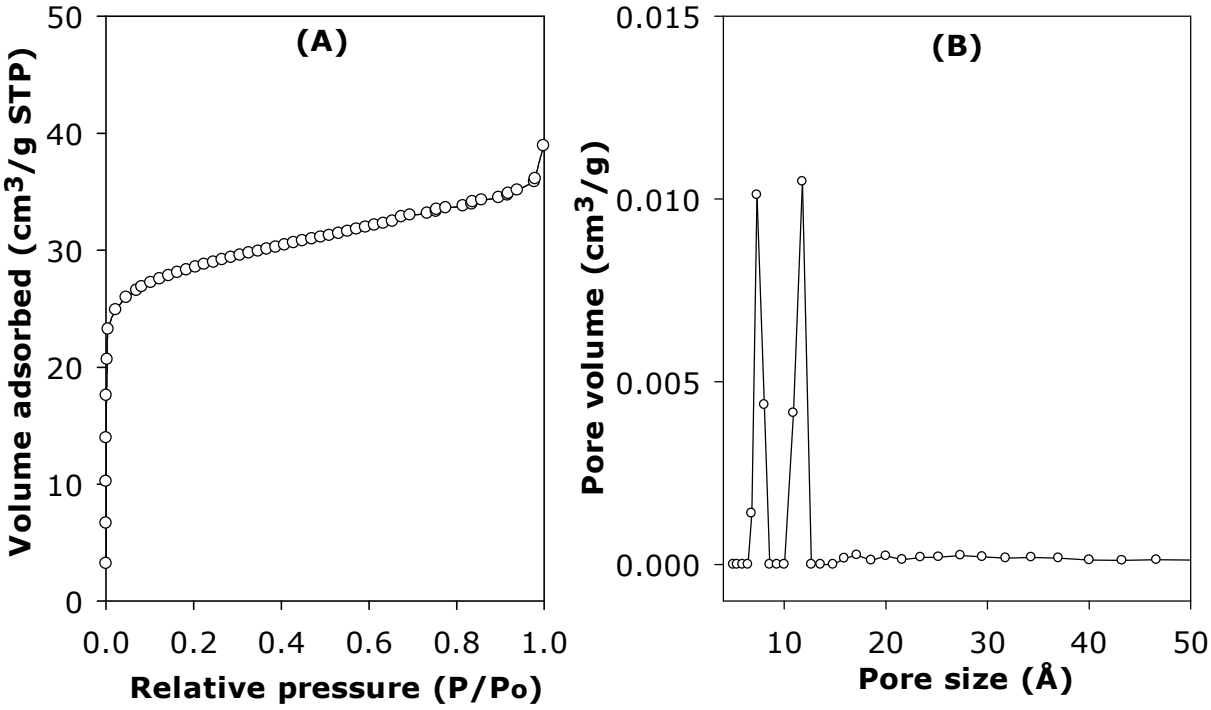


**Supporting Figure S5**. Nitrogen sorption isotherm (A) and pore size distribution curve (B) of CNL1 carbon.

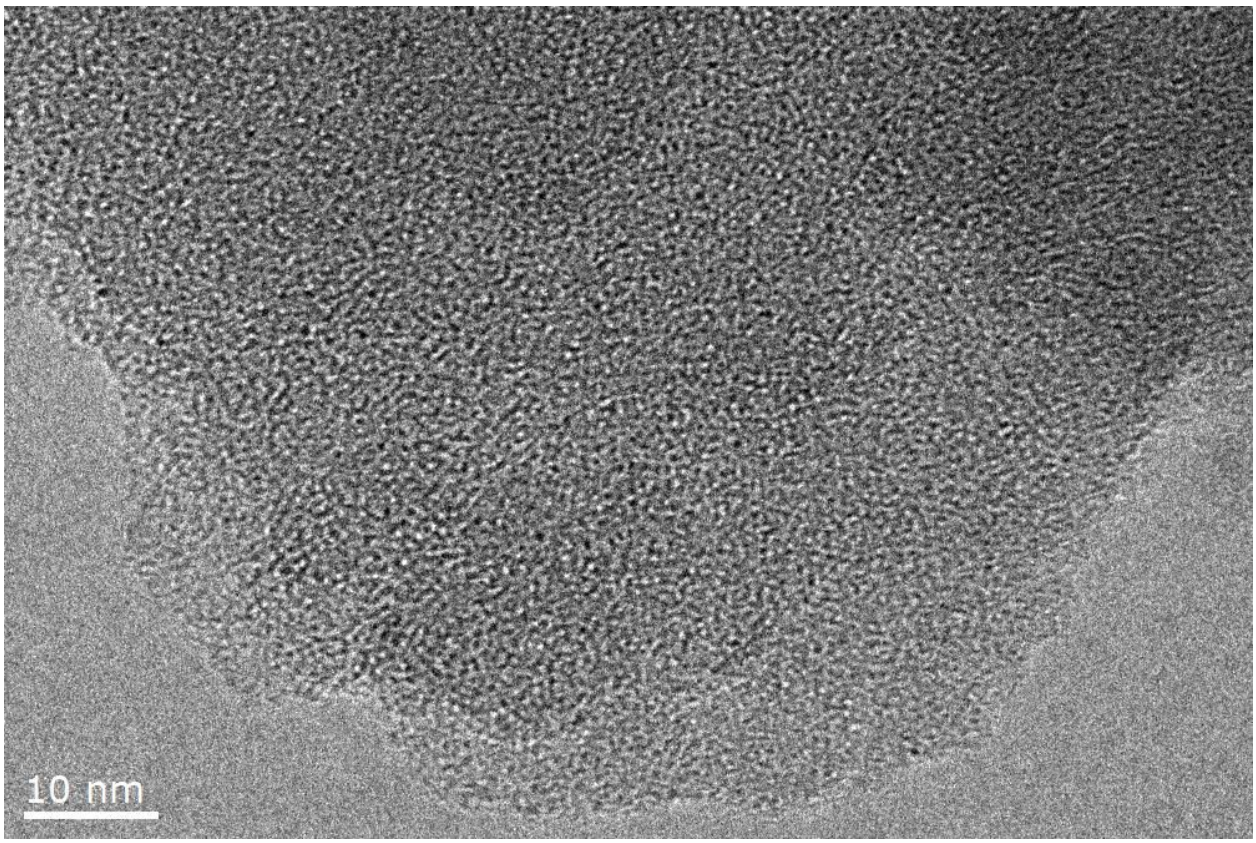


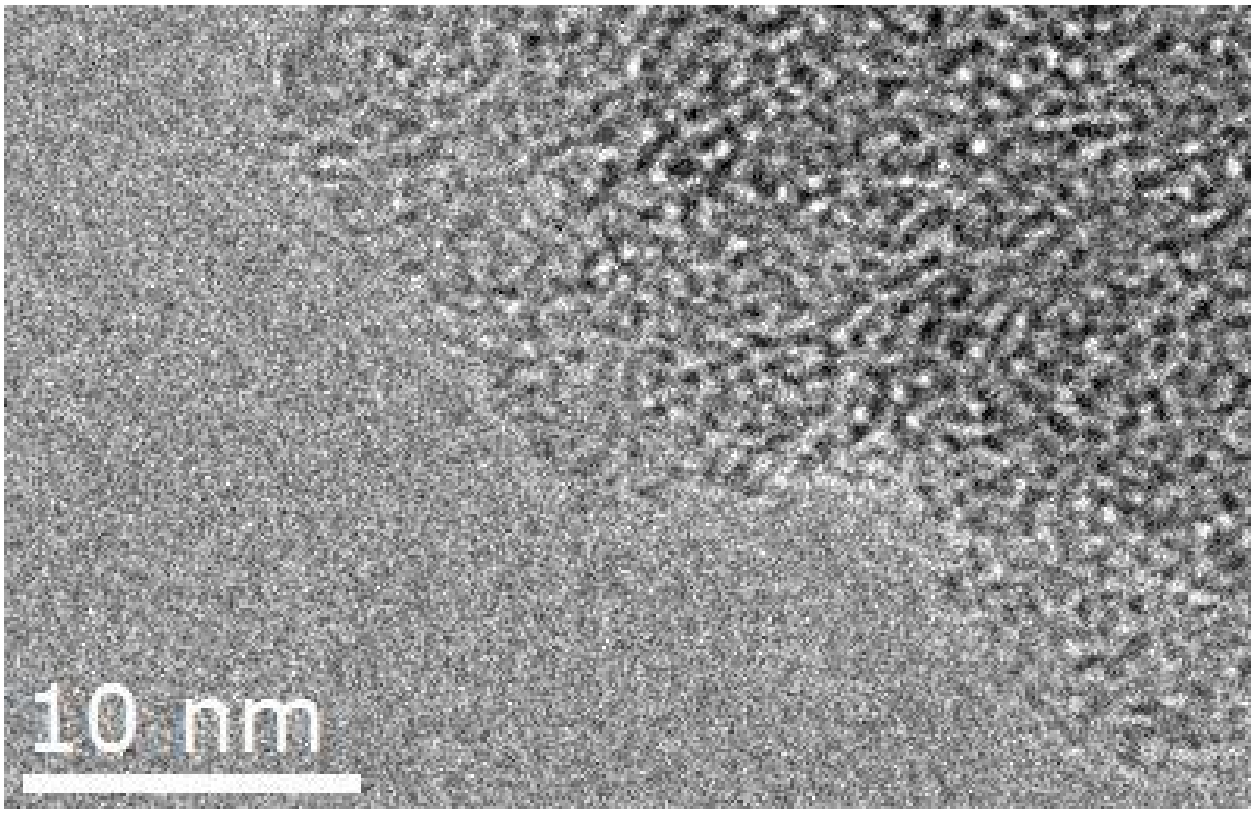


**Supporting Figure S6**. TEM images of CNL1 carbon.

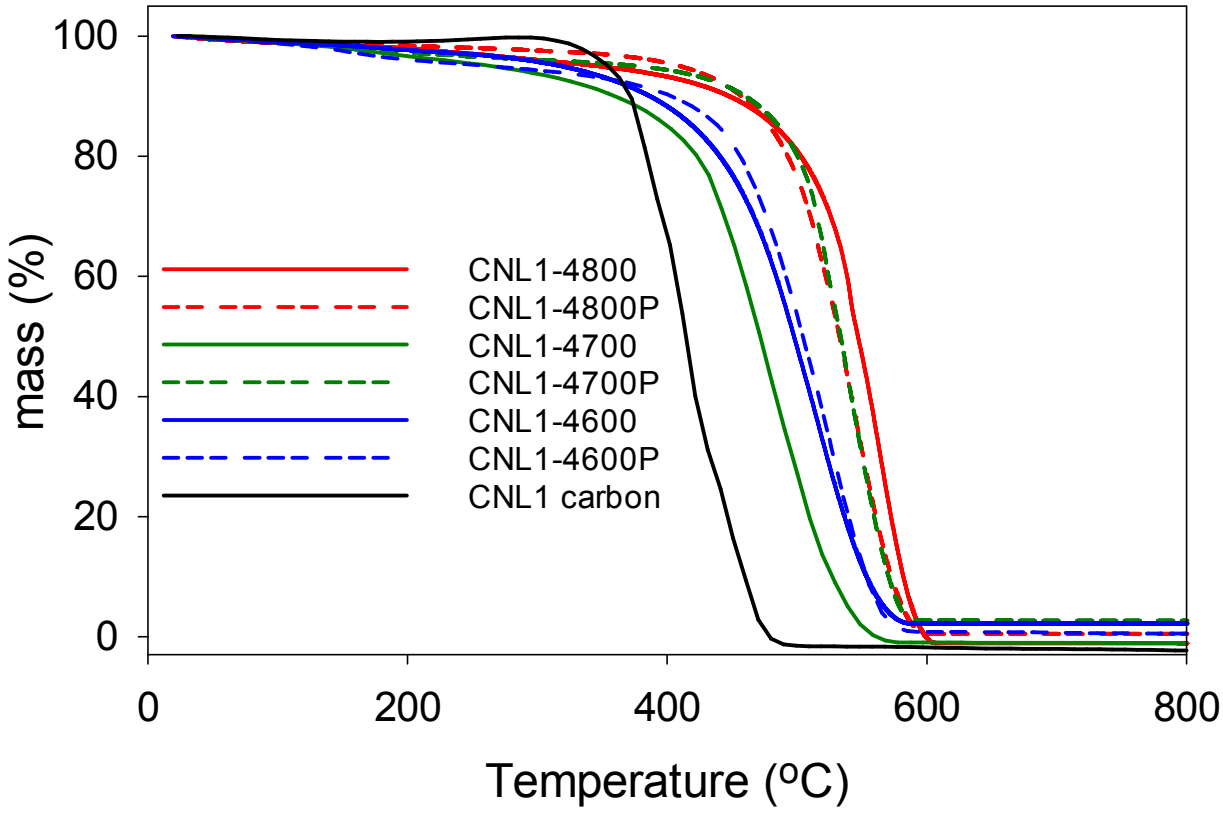


**Supporting Figure S7**. Thermogravimetric analysis (TGA) curve of CNL1 carbon and activated CNL1-4T carbons thermally treated in air.

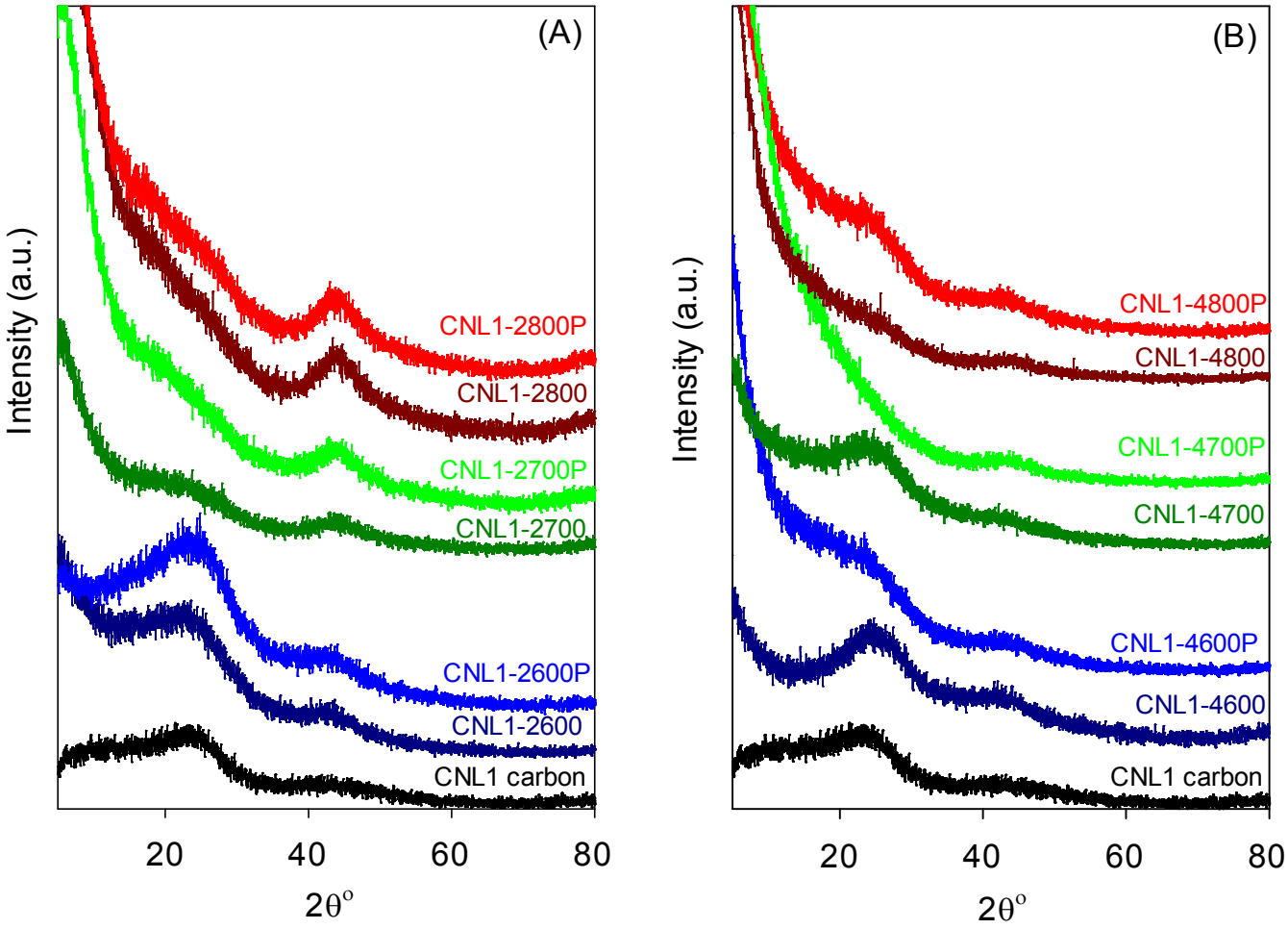


**Supporting Figure S8**. Powder XRD pattern of CNL1 carbon, and activated CNL1-2T (A) and CNL1-4T (B) carbons.

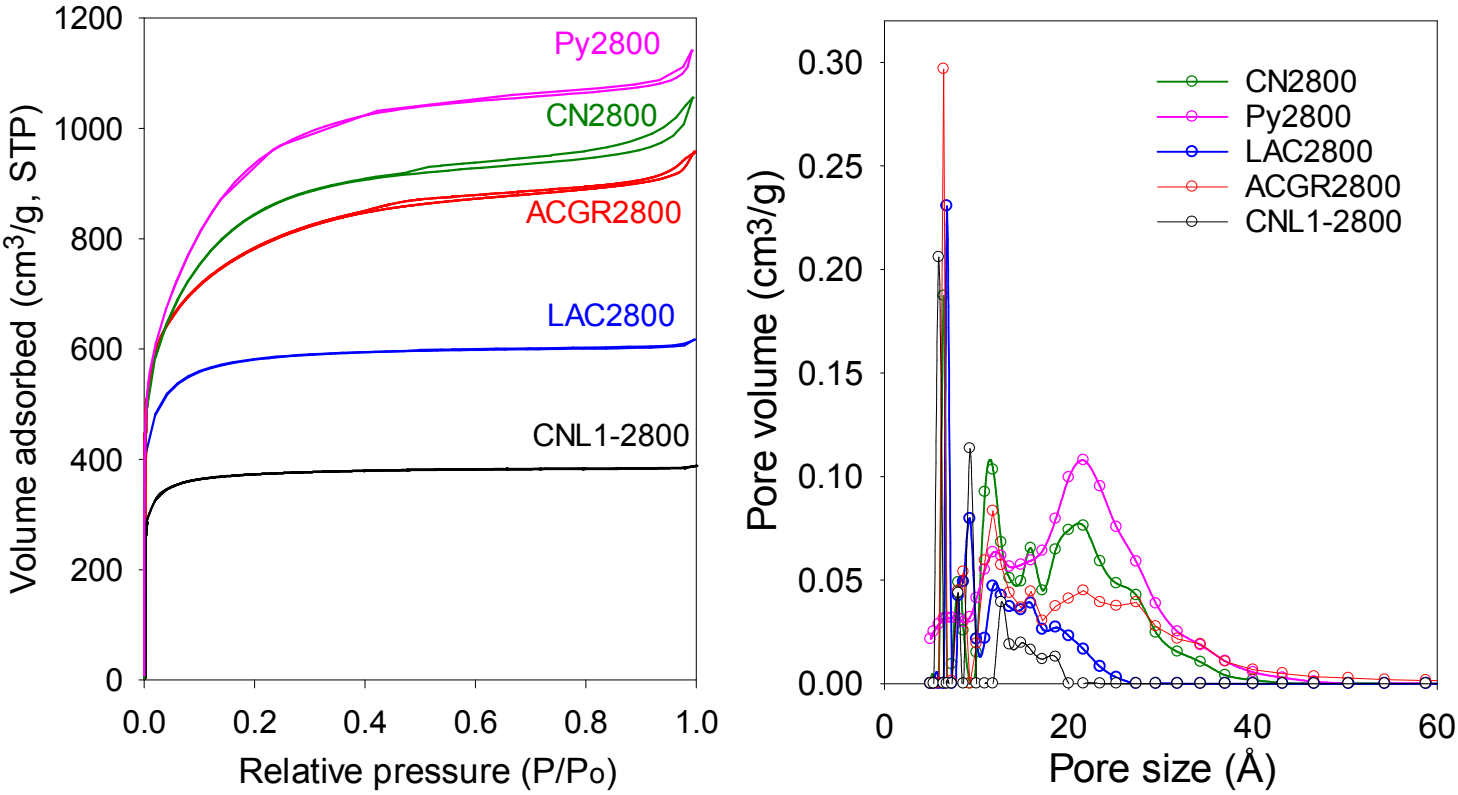


**Supporting Figure S9**. Nitrogen sorption isotherms and pore size distribution curves of activated CNL1-2800 carbon compared to analogous activated carbons derived from lignin (LAC2800), grass (ACGR2800), carbon nanotube superstructures (CN2800) or polypyrrole (Py2800) under similar activation conditions (i.e., 800 ºC and KOH/carbon ratio of 2).

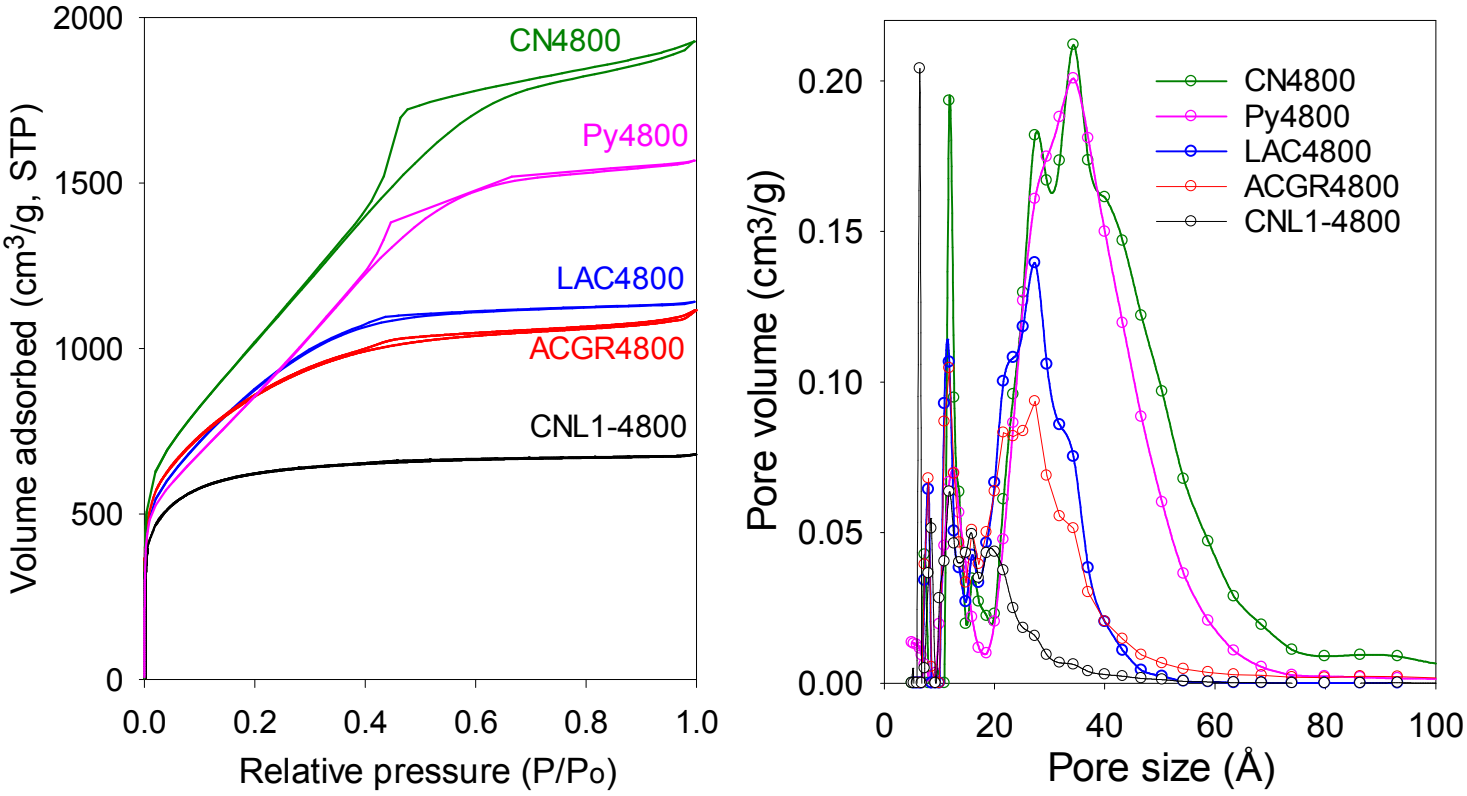


**Supporting Figure S10**. Nitrogen sorption isotherms and pore size distribution curves of activated CNL1-2800 carbon compared to analogous activated carbons derived from lignin (LAC4800), grass (ACGR4800), carbon nanotube superstructures (CN4800) or polypyrrole (Py4800) under similar activation conditions (i.e., 800 ºC and KOH/carbon ratio of 4).

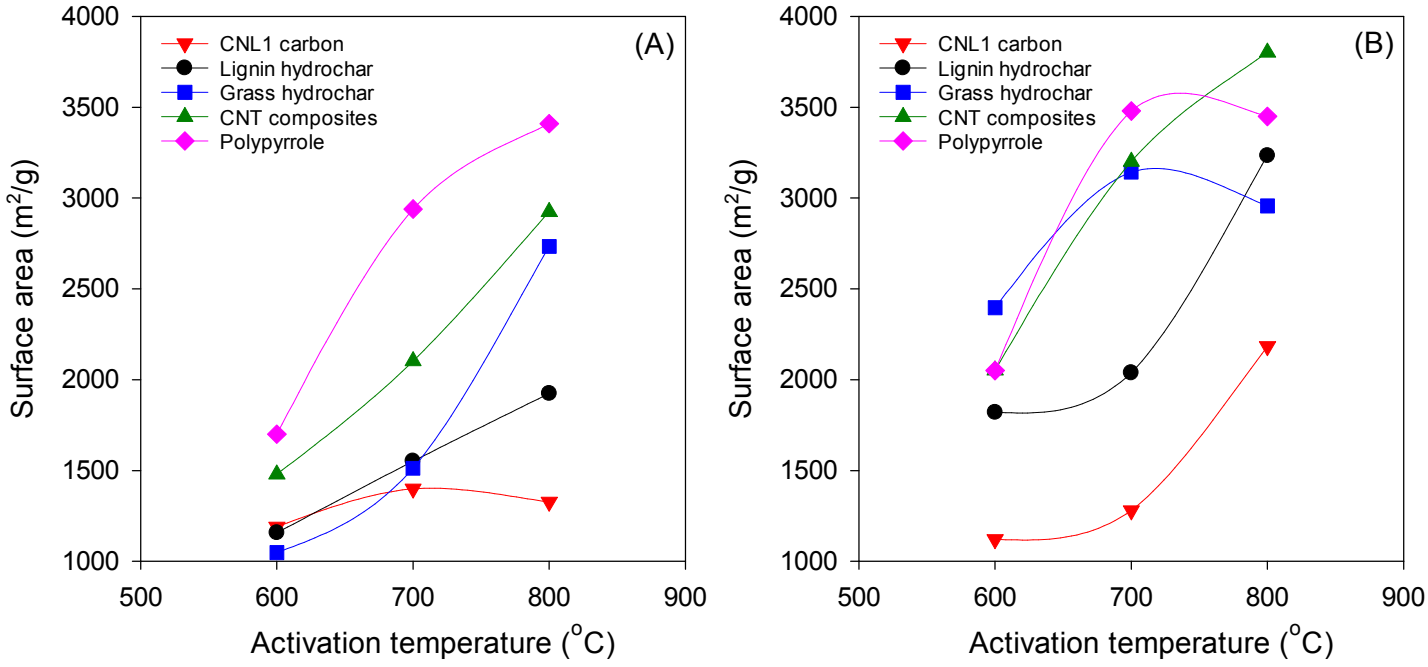


**Supporting Figure S11**. A plot of total surface area as a function of activation temperature for activated carbons derived from CNL1 carbon and other precursors at KOH/carbon ratio of; (A) 2 and (B) 4.

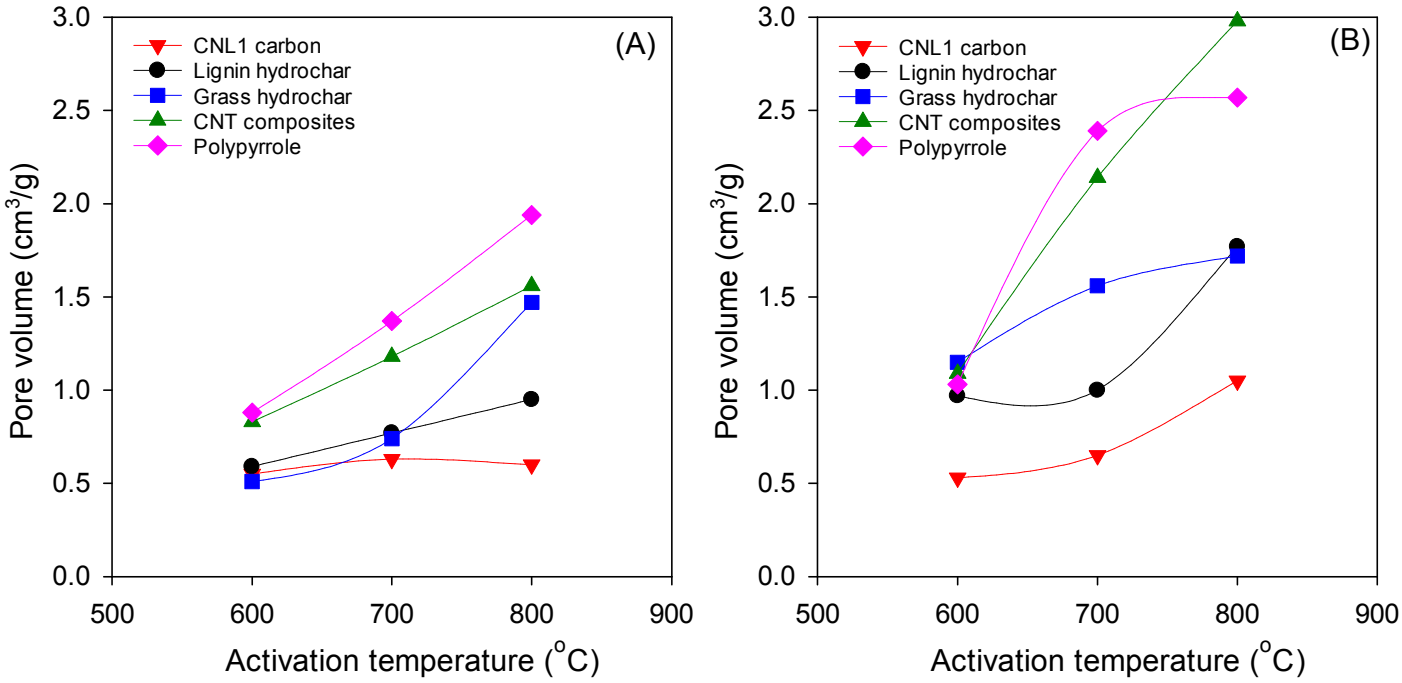


**Supporting Figure S12**. A plot of total pore volume as a function of activation temperature for activated carbons derived from CNL1 carbon and other precursors at KOH/carbon ratio of; (A) 2 and (B) 4.

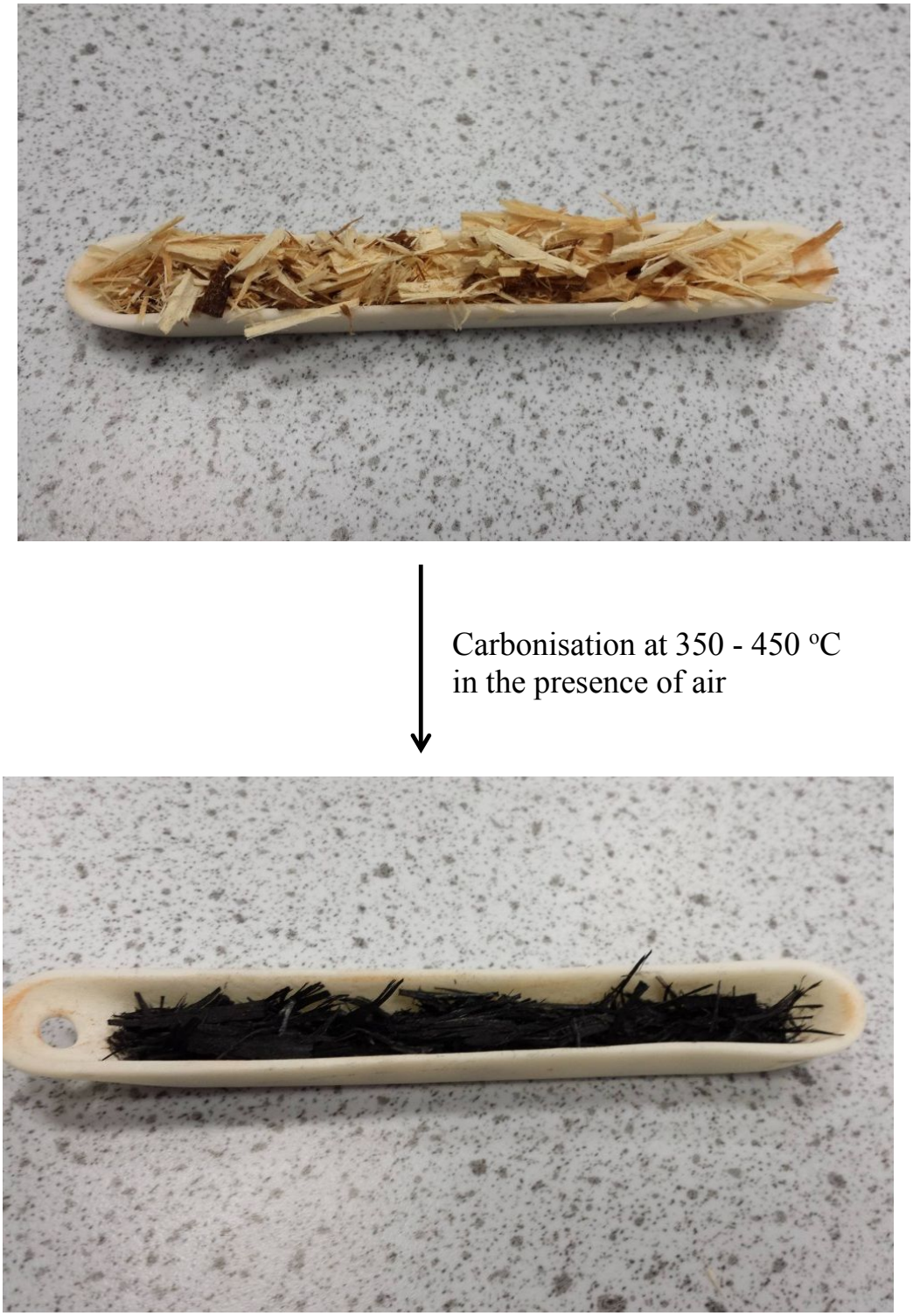


**Supporting Figure S13**. Photographic images of biomass (wood chippings) before (top) and after (bottom) carbonisation in the presence of air.

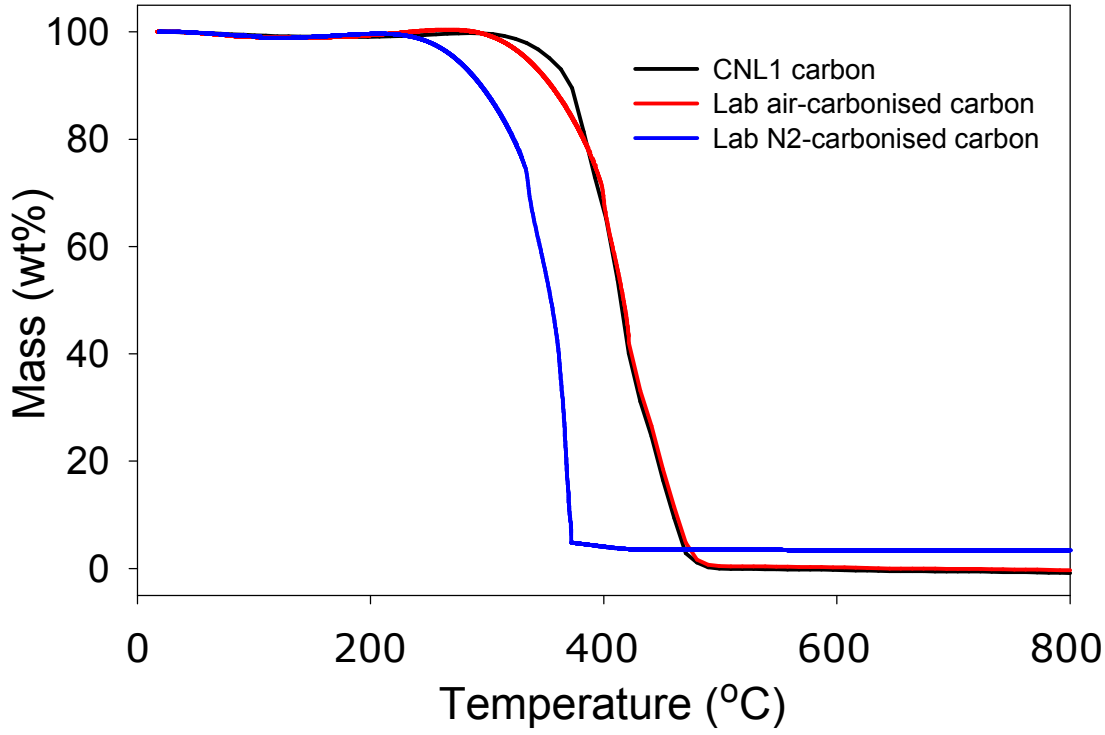


**Supporting Figure S14**. Thermogravimetric analysis (TGA) curve of CNL1 carbon, and lab-based carbon from pyrolysis (carbonisation) of wood chippings under air (lab air-carbonised carbon) or $N_2$ (lab N2-carbonised carbon).

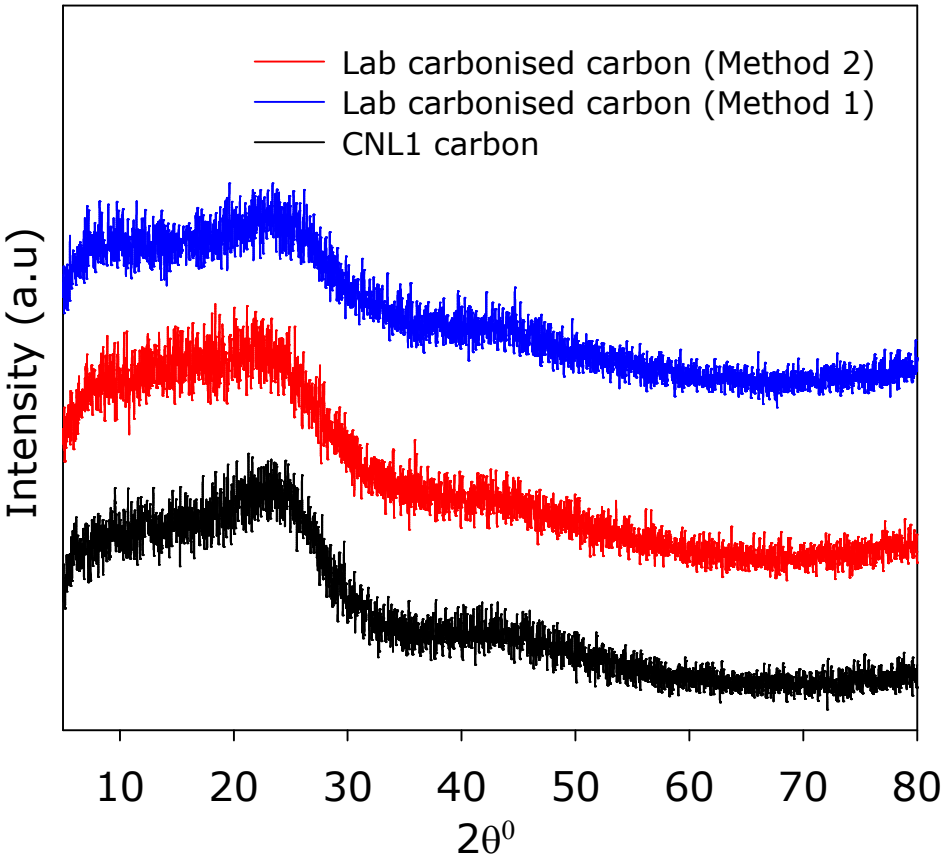


**Supporting Figure S15**. Powder XRD patterns of CNL1 carbon, and lab-based carbon from pyrolysis (carbonisation) of wood chippings under air containing atmosphere. See above for description of method 1 and 2.

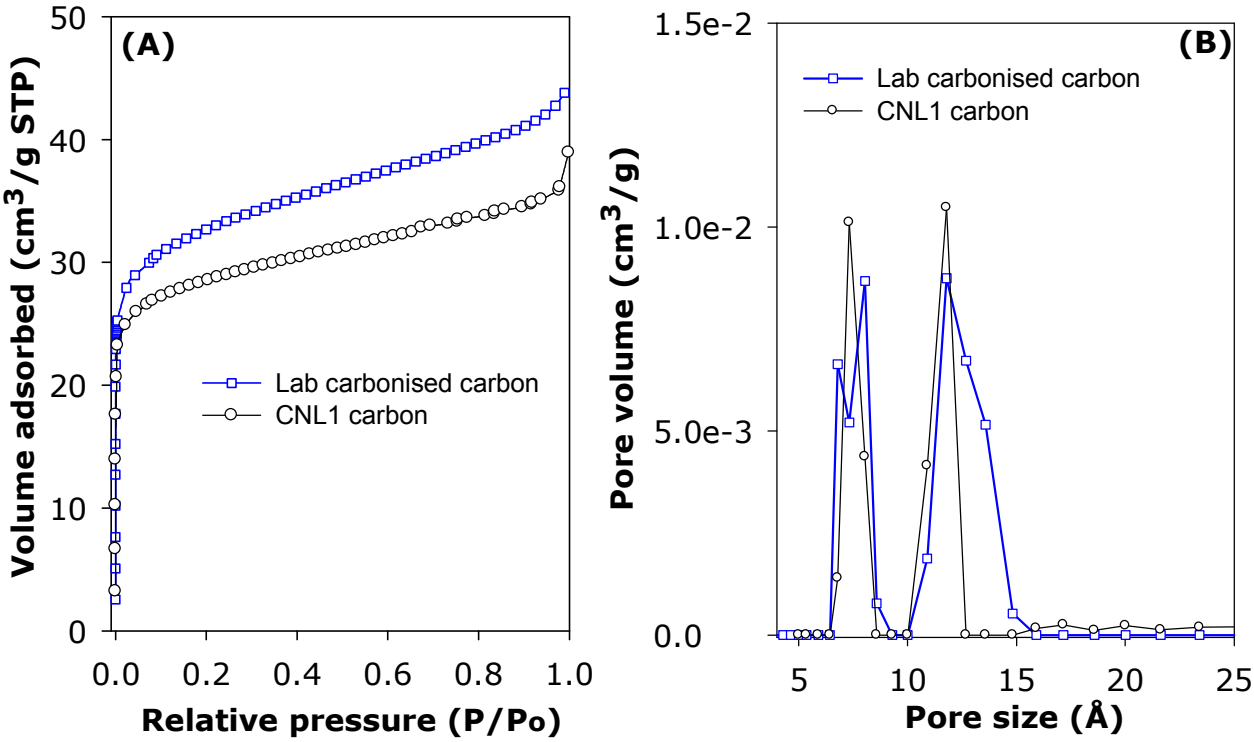


**Supporting Figure S16**. Nitrogen sorption isotherms (A) and pore size distribution curves (B) of CNL1 carbon and lab-based carbon from pyrolysis (carbonisation) of wood chippings under air containing atmosphere.

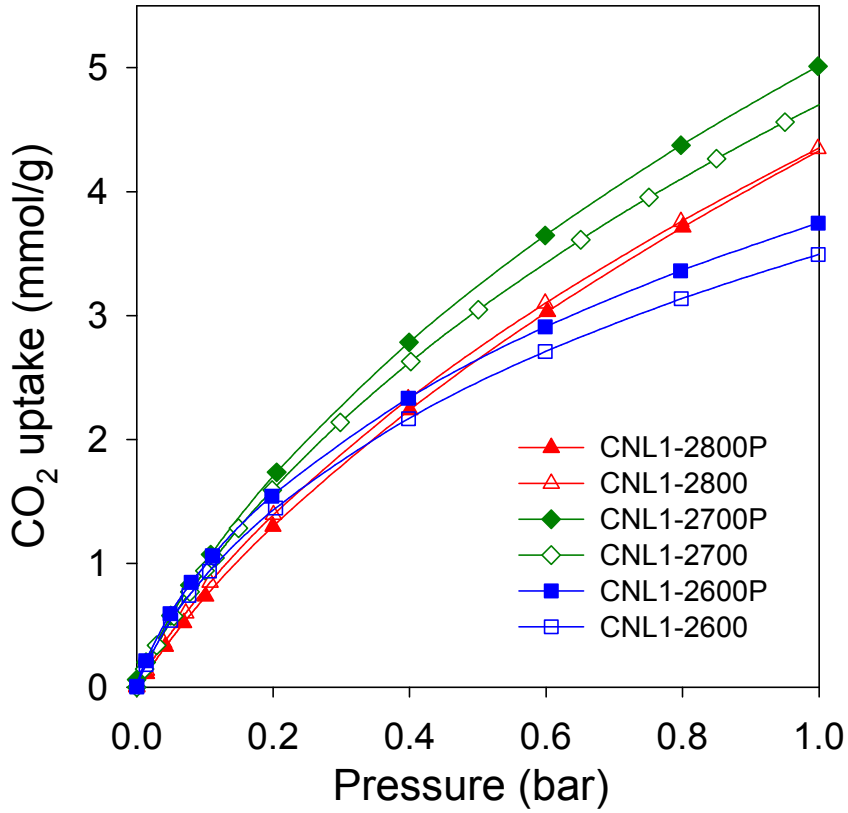


**Supporting Figure S17**. $CO_2$ uptake isotherms at 25 $^{o}$C and 0 - 1 bar for activated CNL1-2T carbons.

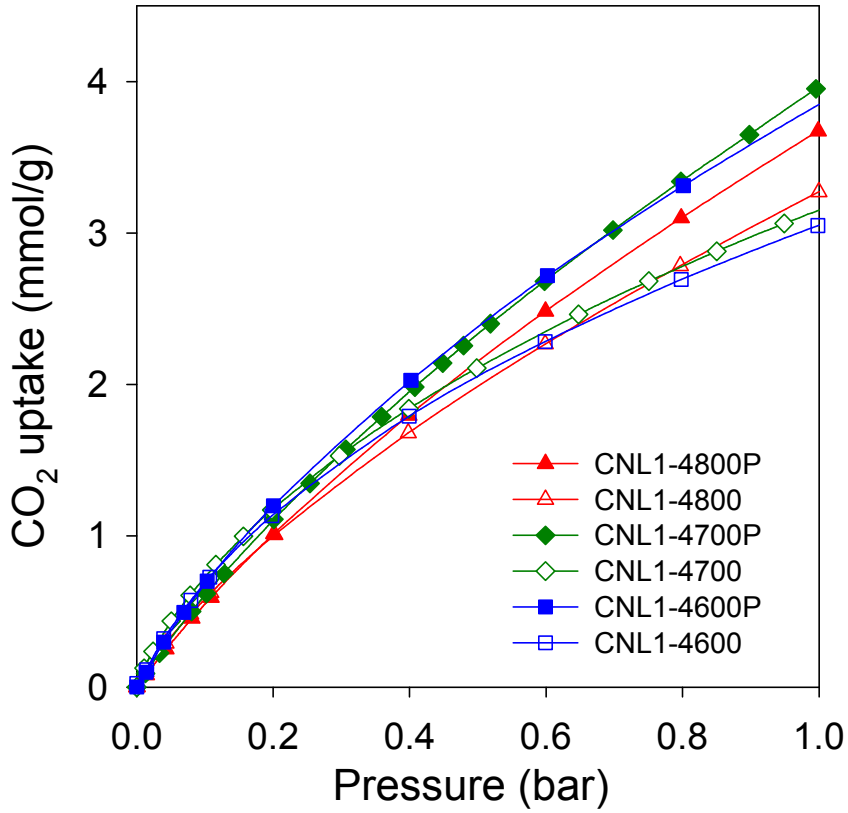


**Supporting Figure S18**. $CO_2$ uptake isotherms at 25 $^{o}$C and 0 - 1 bar for activated CNL1-4T carbons.

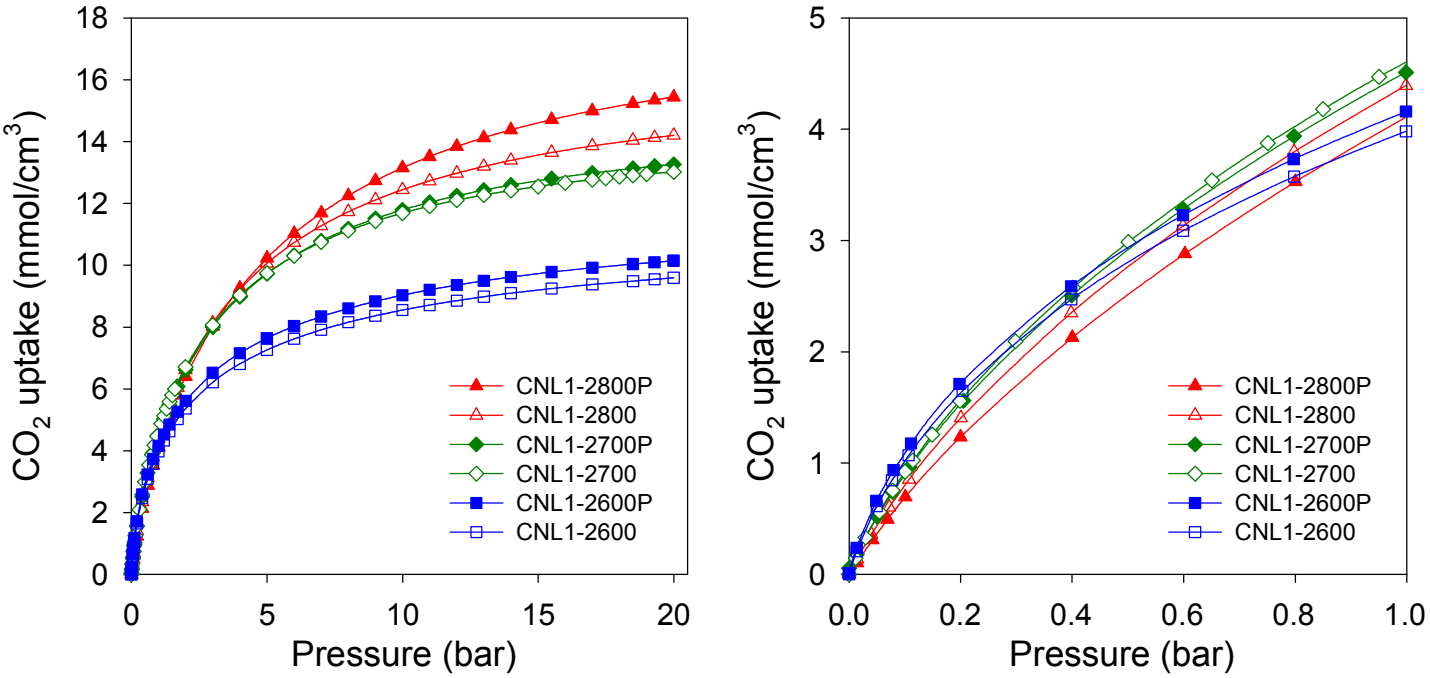


**Supporting Figure S19**. Volumetric $CO_2$ uptake isotherms at 25 ºC and 0 – 20 bar (left panel) and 0 – 1 bar (right panel) for activated CNL1-2T carbons.

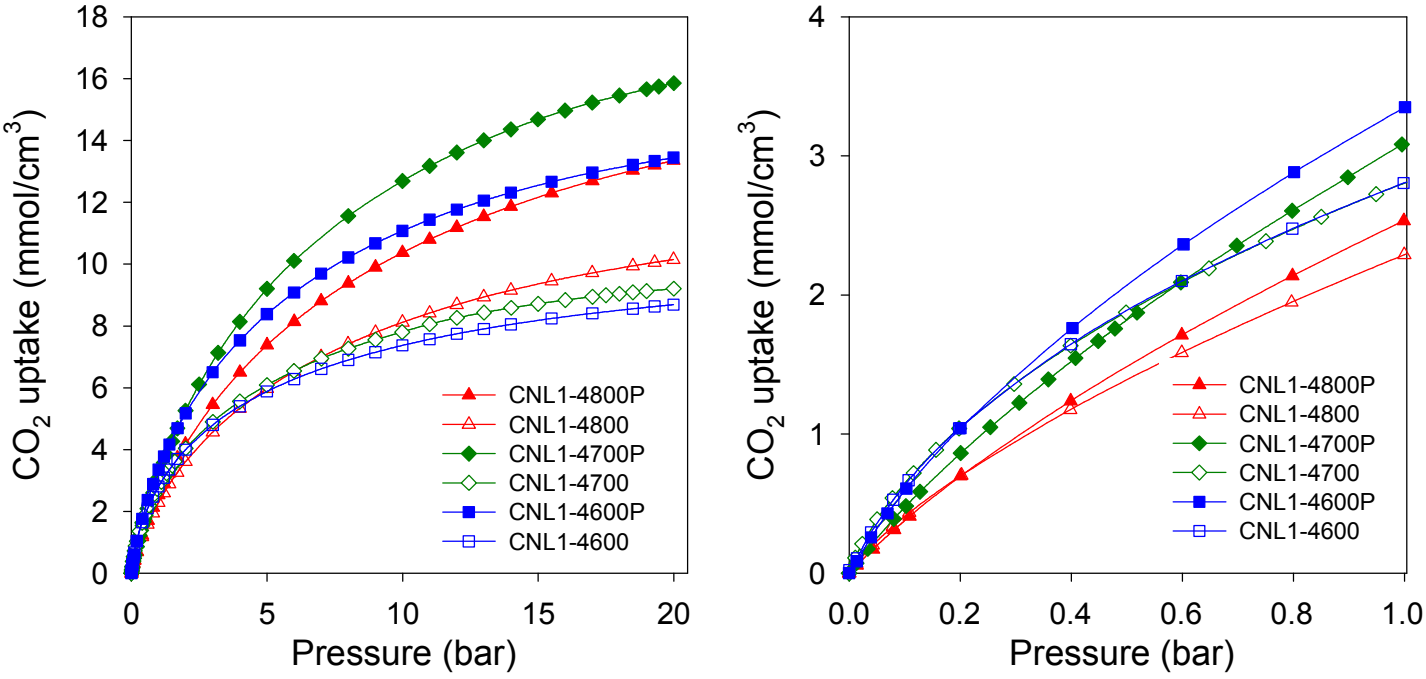


**Supporting Figure S20**. Volumetric $CO_2$ uptake isotherms at 25 ºC and 0 – 20 bar (left panel) and 0 – 1 bar (right panel) for activated CNL1-4T carbons.